Intracellular replication of *Pseudomonas aeruginosa* in epithelial cells requires suppression of the caspase-4 inflammasome

Abby R Kroken[1,2]*, Keith A Klein[2], Patrick S Mitchell[3], Vincent Nieto[1], Eric J Jedel[1], David J Evans[1,4], Suzanne M J Fleiszig[1, 5]

1. Herbert Wertheim School of Optometry & Vision Science, University of California, Berkeley, CA USA
2. Department of Microbiology and Immunology, Loyola University Chicago, Maywood, IL USA
3. Department of Microbiology, University of Washington, Seattle, WA, USA
4. College of Pharmacy, Touro University California, Vallejo, CA USA
5. Graduate Groups in Vision Sciences, Microbiology, and Infectious Diseases & Immunity, University of California, Berkeley, CA USA

* Corresponding author. Department of Microbiology and Immunology, Loyola University Chicago, Maywood, IL, USA. Email: akroken@luc.edu

Abstract

Pathogenesis of *Pseudomonas aeruginosa* infections can include bacterial survival inside epithelial cells. Previously, we showed this involves multiple roles played by the type three-secretion system (T3SS), and specifically the effector ExoS. This includes ExoS-dependent inhibition of a lytic host cell response that subsequently enables intracellular replication. Here, we studied the underlying cell death response to intracellular *P. aeruginosa*, comparing wild-type to T3SS mutants varying in capacity to induce cell death and that localize to different intracellular compartments. Results showed that corneal epithelial cell death induced by intracellular *P. aeruginosa* lacking the T3SS, which remains in vacuoles, correlated with activation of NF-κB as measured by p65 relocalization and TNFα transcription and secretion. Deletion of caspase-4 through CRISPR-Cas9 mutagenesis delayed cell death caused by these intracellular T3SS mutants. Caspase-4 deletion also countered more rapid cell death caused by T3SS effector-null mutants still expressing the TSSS apparatus that traffic to the host cell cytoplasm, and in doing so rescued intracellular replication normally dependent on ExoS. While HeLa cells lacked a lytic death response to T3SS mutants, it was found to be enabled by interferon gamma treatment. Together, these results show that epithelial cells can activate the noncanonical inflammasome pathway to limit proliferation of intracellular *P. aeruginosa*, not fully dependent on bacterially-driven vacuole escape. Since ExoS inhibits the lytic response, the data implicate targeting of caspase-4, an intracellular pattern recognition receptor, as another contributor to the role of ExoS in the intracellular lifestyle of *P. aeruginosa*.

Author Summary

Pseudomonas aeruginosa can exhibit an intracellular lifestyle within epithelial cells in vivo and in vitro. The type three secretion system (T3SS) effector ExoS contributes via multiple mechanisms, including extending the life of invaded host cells. Here, we aimed to understand the underlying cell death inhibited by ExoS when *P. aeruginosa* is intracellular. Results showed that intracellular *P. aeruginosa* lacking T3SS effectors could elicit rapid cell lysis via the non-canonical inflammasome pathway. Caspase-4 contributed to cell lysis even when the intracellular bacteria lacked the entire T33S and were consequently unable to escape vacuoles, representing a naturally occurring subpopulation during wildtype infection. Together, the data show the caspase-4 inflammasome as an epithelial cell defense against intracellular *P. aeruginosa*, and implicate its targeting as another mechanism by which ExoS preserves the host cell replicative niche.

Introduction

Pseudomonas aeruginosa is an important human opportunistic pathogen, able to cause both life- and sight-threatening infections in multiple body sites. While often referred to as an extracellular pathogen, *P. aeruginosa* can adopt an intracellular lifestyle in various epithelial cell types, including corneal [1], bronchial [2], HeLa cells [3] and in vivo [4]. Research published by us and others has shown that the ability of *P. aeruginosa* to persist/replicate inside a host cell depends on the type three secretion system (T3SS), with multiple roles played by the T3SS effector ExoS [5-7] encoded by only invasive strains [8].

ExoS is a bifunctional protein with both RhoGAP and ADP ribosyltransferase (ADPr) activity, and the broad substrate specificity of its ADPr domain [9, 10] enables ExoS to impact multiple host processes [11, 12]. Demonstrated effects of ExoS include inactivation of host cell proliferative/survival signaling, disassembling the host cell cytoskeleton, freezing of intracellular membrane trafficking, and disruption of ROS generation [9, 13-16]. While the molecular components of host cells targeted by ExoS to enable *P. aeruginosa* to persist intracellularly have not yet been elucidated, its ADPr activity is required, and the mechanisms shown include both inhibition of autophagy [17] and evasion of lysosomes [18]. Recently, we reported another role for the ADPr activity of ExoS in intracellular persistence by *P. aeruginosa*; the preservation of host cell viability [19], which was further explored here.

Eukaryotic host cells can generally sense and respond to invasion by intracellular pathogens [20, 21]. Responses can include initiation of regulated cell death pathways [22], which may

74 subsequently be suppressed by the bacteria to preserve their intracellular niche [23]. An example
75 of this death response is pyroptosis, a form of lytic cell death that tends to be inflammatory [20].
76 Multiple pyroptotic pathways have been identified, each sensing different pathogen-associated
77 molecular patterns (PAMPs) [24-27] or pathogen-associated aberrant activities [28, 29]. The
78 sensor then converges on the activation of a cysteine-aspartic protease: caspase-1 for canonical
79 inflammasome pathways [30, 31], and caspase-4/5 for later-discovered pathways designated
80 noncanonical [32-34]. Inflammatory caspases cleave and activate gasdermin D [35, 36], which
81 assembles into pores in host plasma membranes [37]. This leads to release of cytokines [38], and
82 total lysis for many cell types [39]. Caspase-1 can also process cytokines IL-18 and IL-1β into
83 mature forms [40], which are secreted through gasdermin D pores or released after cell lysis [35].
84
85 *P. aeruginosa* effectors ExoS and ExoT can reduce IL-1β secretion in macrophages [41-43],
86 suggesting inflammasome interference might occur. However, responses of macrophages and
87 epithelial cells can differ, and while inflammasome function has been well-studied in macrophages
88 and other myeloid cells, the repertoire of inflammasomes shown in epithelial cells (e.g. corneal
89 epithelial cells) is more limited, and functions less-well understood [44]. One inflammasome
90 pathway studied in some corneal diseases and cultured cells is NLRP3 [45, 46], which can detect
91 numerous stimuli [47] including ionic flux from pore formation [48], lysosomal damaging agents
92 [49], and bacterial RNA [50]. However, not all relevant studies verified which corneal cell type
93 expressed NLRP3, or explicitly determined if NLRP3 was activated, versus other inflammasome
94 pathways that could also yield mature IL-1β secretion. Recently, both caspase-4 (detects
95 cytoplasmic LPS [51]) and NLRP1 (detects pathogenic enzymatic activities and dsRNA [28, 52])
96 were shown to be expressed and functional in the human corneal epithelium [53, 54]. The Protein

97 Atlas RNAseq data set for the corneal epithelial limbal stem cell line hTCEpi [55] provides
98 evidence for expression of caspase-4, caspase-5 (an additional LPS sensor [33, 56]), NLRP1, and
99 NLRC4 (although its required sensor protein NAIP [57] was not detected) [58]. While NLRP3,
100 Pyrin, and AIM2 inflammasomes were not detected in the hTCEpi cell line, this does not preclude
101 upregulation upon specific stimuli, or in the context of corneal tissue in vivo [58].
102
103 Having shown that the T3SS effector ExoS inhibits rapid cell lysis induced by intracellular *P.*
104 *aeruginosa* [19], in this study we investigated the mechanisms underlying host cell death elicited
105 and modulated by intracellular *P. aeruginosa*. In doing so, we leveraged the finding that *P.*
106 *aeruginosa* mutants lacking the entire T3SS (Δ*exsA* mutants) remain toxic to corneal epithelial
107 cells [59], contrasting with HeLa and CHO cells [60, 61]. Results showed that caspase-4 is required
108 for corneal epithelial cell death in response to *P. aeruginosa* invasion, and in this way limits
109 accumulation of an intracellular population of bacteria. While caspase-4-dependent death occurred
110 even if bacteria lacked the ability to leave vacuoles/enter the cytoplasm, the response was faster
111 when they could. Moreover, the death response was enabled in otherwise unresponsive (HeLa)
112 cells after stimulation with interferon gamma, which has been shown to limit cytoplasmic sub-
113 populations of *Salmonella* within HeLa cells in a manner dependent on Caspase-4 and GBP
114 proteins [62]. Since ExoS inhibits the cell death response to intracellular *P. aeruginosa*, these
115 results implicate ExoS targeting of a caspase-4 dependent response as another contributor to its
116 well-established role in intracellular survival by *P. aeruginosa*.
117
118 **Results**
119

120 ***P. aeruginosa* lacking the T3SS kill corneal epithelial cells but not HeLa cells.**

121 Generally, it is thought that *P. aeruginosa* mutants missing the T3SS (i.e., Δ*exsA* mutants) do not
122 cause lytic death of cultured epithelial cells, as shown for HeLa and CHO cells [60, 61]. However,
123 our published work has shown that Δ*exsA* mutants are able to kill corneal epithelial cells, with
124 contributions made by the intracellular population [59]. Recognizing that differences between cell
125 types could potentially assist in deciphering mechanisms, we directly compared corneal epithelial
126 cells (hTCEpi) [55] to HeLa cells using the same methods. Impact of wild type PAO1, Δ*exsA*
127 mutants (lacking the entire T3SS), and Δ*exoSTY* mutants (lacking all known T3SS effectors) were
128 studied. After a 3-hour invasion period, extracellular bacteria were eliminated using the non-cell
129 permeable antibiotic amikacin [3]. Cell death rates were measured with a FIJI macro that counts
130 propidium iodide-positive nuclei (permeabilized cells) and Hoechst-labeled nuclei (total cells) and
131 reports a ratio over a 20-hour post-infection period [19]. The results confirmed that the two cell
132 types were differentially susceptible. Death rates for corneal epithelial cells were statistically
133 similar for wild type and Δ*exsA* mutants (**Figure 1A-B**), whereas HeLa cells infected with Δ*exsA*
134 mutants showed very little cell death even at the 20-h post infection time point when most corneal
135 epithelial cells had died (**Figure 2C-D**). In both cell types, the Δ*exoSTY* mutant yielded the most
136 rapid cell death as noted previously [19]. Thus, corneal epithelial cells have an intrinsic response
137 to T3SS-null bacteria that is absent in HeLa cells, which may underly cell death occurring in
138 response to T3SS-positive bacteria.

139

140 **Cell death from T3SS-null mutants is driven by live, culturable intracellular bacteria.**

141 In a previous study we demonstrated that the corneal epithelial cell death response to Δ*exsA*
142 mutants depends on intracellular bacteria, using the cell-permeable antibiotic ofloxacin to suppress

143 them [59]. Results showed that host cell death was reduced in a dose dependent fashion by
144 ofloxacin compared to untreated controls. Importantly, in both test and control samples, the
145 extracellular bacteria had already been killed using a non-cell permeable antibiotic before studying
146 the impact of intracellular populations. Still unknown was whether the killed extracellular bacteria
147 contributed to triggering host cell death measured at a later time point. To address this, Δ*exsA*
148 mutants were killed using multiple strategies before challenging cells. Because live bacteria
149 replicate in tissue culture media during the 3-hour invasion period, MOIs that approximated
150 bacterial numbers two or three hours post infection (i.e., 160 or 640) were also tested. Neither heat-
151 killed nor paraformaldehyde-fixed bacteria induced corneal epithelial cell cytotoxicity (**Figure**
152 **2A, B**). However, bacteria killed using antibiotic (amikacin), caused a small but still detectable
153 cell death response that was independent of MOI. (**Figure 2C**). Potentially explaining that result,
154 visual observation during time lapse configuration revealed a small fraction of amikacin-treated
155 bacteria that continued to display swimming motility (**Supplemental Movie 1**) despite not being
156 recoverable by culturing on TSA agar, suggesting transient persisters retaining some functional
157 capacities remained present in the assay. Bacteria were exposed to amikacin for a longer time
158 period (3 hours), prior to inoculating corneal epithelial cells, although this did not change the
159 experimental outcome (**Figure 2D**). Thus, extracellular amikacin-killed bacteria may contribute
160 to the death of a sub population of host cells in our experimental system, however live bacteria
161 lead to greater host cell death rates, much of which is attributed to intracellular bacteria [59].
162

163 **Dynamics of cell death in only bacterially-occupied cells confirms roles for both T3SS**
164 **machinery and T3SS effectors.**

165 Visual inspection of infected cells suggested that not all cells were occupied by bacteria, and that
166 some apparently non-occupied cells also died. Recognizing that this could skew results in bulk
167 analyses of cell death rates, we performed additional experiments to consider only bacterially-
168 occupied cells in our analyses. To enable this, we employed methods that allowed simultaneous
169 detection of viable intracellular bacteria and host cell [19]. To monitor timing of lytic cell death
170 we used propidium iodide, which labels the nucleus only if the host cell membrane becomes
171 permeabilized. Wild type (PAO1) was compared to mutants lacking the entire T3SS (Δ*exsA*
172 mutants), and Δ*exoSTY* mutants lacking only T3SS effectors, using quantitative time lapse imaging
173 over 20 h. Since Δ*exsA* mutants do not kill HeLa cells, this analysis was only done using corneal
174 epithelial cells.
175
176 To detect Δ*exsA* mutants inside cells, we previously used an arabinose-inducible green fluorescent
177 protein (GFP) expression vector pBAD-GFP [59]. This adaptation of a method originally described
178 for monitoring viability of intracellular *Salmonella* (29) involves induction of GFP expression
179 using arabinose induction only after bacteria have invaded cells and extracellular populations are
180 killed (using amikacin). In an attempt to keep experimental methods consistent across samples, we
181 explored the feasibility of using the induction method to also study wild type and the Δ*exoSTY*
182 mutants. Unfortunately, fewer bacterial cells exhibited cytoplasmic spread using the arabinose
183 induction method compared to our previously used T3SS reporter method (**Supplemental Figure**
184 **1A**). Moreover, while the host cell death rate was similar for wild type PAO1 using both methods,
185 it trended lower for Δ*exoSTY* mutants expressing arabinose-induced GFP (**Supplemental Figure**
186 **1B)**. This suggested GFP induction in this context impacts the T3SS or some other components of
187 the intracellular pathway relevant to cytoplasmic entry or spread, a step important for intracellular

188 infection by wild type and Δ*exoSTY* mutants, but not for Δ*exsA* mutants (which cannot escape
189 vacuoles due to lack of the T3SS). Indeed, T3SS effector secretion was found reduced *in vitro*
190 using EGTA stimulation in the presence of arabinose only when bacteria were transformed with
191 pBAD-GFP (**Supplemental Figure 1C**). Thus, the T3SS expression plasmid pJNE05 was used to
192 study wild type and Δ*exoSTY* mutants, reserving the arabinose induction pBAD-GFP method for
193 studying the Δ*exsA* mutant which cannot be visualized using the T3SS expression system.
194
195 Images from a typical 20 h time-lapse experiment using Δ*exsA* mutants are shown in **Figure 3A**.
196 As expected, Δ*exsA* mutants localized to vacuoles inside cells [59]. Most bacteria-occupied cells
197 died before the end of the 20 h assay, as shown by propidium iodide labeling of the nucleus. On
198 the other hand, **Figure 3B** shows an invaded cell still alive at 20 hours (no propidium iodide
199 labeling), representing a minority of cells at this time point. Videos of these time lapse experiments
200 are available in **Supplemental Movie 2**, which includes cells visualized in **Figures 3B and 3C** at
201 20 hours post infection. As expected, both wild type PAO1 and Δ*exoSTY* mutant infected cells
202 (shown in **Figure 3D)** replicated in the host cell cytoplasm after bacterial escape from vacuoles
203 [19]. In both cases, most occupied cells died by the end of the assay, the Δ*exoSTY* mutant doing
204 so even more rapidly, expected due to lack of ExoS which normally counters cell death [19].
205 Importantly, propidium iodide labeling (lytic cell death) preceded the loss of the GFP signal from
206 intracellular bacteria, which was replaced with propidium iodide positive bacterial bodies (**Figure**
207 **3C and Supplemental Movie 2)**. Given that lytic cell death allows the non-cell permeable
208 antibiotic used in these assays to enter cells, the bacterial GFP signal loss shortly after cell lysis
209 confirmed that labeled bacteria had been inside a cell with an intact plasma membrane, and were
210 not simply antibiotic resistant extracellular bacteria.

211

212 A computational approach was used to quantitatively assess the timing of when populations of
213 invaded cells died [19], and a super violin plot visualization script developed by Kenny and Schoen
214 was used to show biological replicates in single plots [63]. This analysis confirmed quantitatively
215 that intracellular Δ*exsA* mutants killed their occupied cells at a broad range of time points.
216 However, the mean value of invaded cell survival times was unexpectedly similar to wild type
217 PAO1 (**Figure 3E**). The analysis also confirmed that the intracellular Δ*exoSTY* mutant infections
218 caused cell lysis at a more rapid rate, significantly different from both wild type PAO1 and Δ*exsA*
219 mutants [19]. Thus, while cell death can be driven by vacuolar contained bacteria, it was more
220 rapid if they could access the cytoplasm while lacking effectors/ExoS able to counter cell death.

221

222 **T3SS-null mutant bacteria engage NF-κB signaling in corneal epithelial cells**.

223 To explore molecular mechanisms involved in *P. aeruginosa*-driven cell death in these assays, a
224 real time PCR array with selected genes involved in regulated cell death pathways was used to
225 study candidate host responses. Corneal cells and HeLa epithelial cells were infected with wild
226 type PAO1, Δ*exoSTY* mutants or Δ*exsA* mutants. Results showed that TNFα and BCL2A1 were
227 upregulated in excess of fifty-fold in both cell lines: (**Figure 4**). In the corneal cells, wild type and
228 both mutants upregulated these genes, while in HeLa cells, only the PAO1Δ*exoSTY* mutant had
229 that impact.

230

231 Since TNFα and BCL2A1 can be regulated by NF-κB signaling, activation of NF-κB was
232 measured at the single-cell level by observing translocation of p65 to the nucleus (**Figure 5A**). In
233 corneal epithelial cells, infection with each tested strain caused p65 translocation, correlating with

234 positive target gene transcription. In HeLa cells, only infection with Δ*exoSTY* mutants led to p65
235 translocation (**Figure 5B)**. The result with wild type PAO1 infection was difficult to discern due
236 to cell rounding; however, p65 appeared excluded from the nuclear portion of HeLa cells (**Figure**
237 **5B, inset)**. Overall, nearly every cell in the population showed similar p65 localization, despite
238 fewer than half of cells being invaded in this experimental system [3]. This finding correlated with
239 the transcriptional data, and is suggestive of a mechanism in which the T3SS effectors limit p65
240 translocation in HeLa cells, but not corneal epithelial cells.
241
242 Since TNFα is associated with both apoptotic and necrotic cell death, TNFα secretion from
243 infected cells was measured by ELISA. The results showed that while wild type PAO1 stimulated
244 TNFα secretion from corneal epithelial cells, higher levels were detected after infection with the
245 Δ*exoSTY* mutant, and the Δ*exsA* mutant causing an intermediate response (**Figure 4B**).
246
247 Having found TNFα secretion levels correlated with cell death rates, we next asked if there was a
248 direct causative relationship that might also explain why some cells without visible intracellular
249 bacteria could also be killed. Thus, the media from naïve cells or Δ*exsA* mutant-infected cells was
250 replaced with filter-sterilized media from Δ*exoSTY* mutant-infected cells (high TNFα). The
251 outcome showed that this did not enhance host cell death rates (**Figure 4C**), suggesting cell death
252 is not driven by a secreted factor such as TNFα, and requires extracellular bacteria, at a minimum
253 (**Figure 2**).
254
255 **Caspase-4 is involved in cell death response to intracellular *P. aeruginosa*.**

256 The morphology of dying cells included membrane integrity loss, intact nucleus, and transient
257 blebbing, all suggestive of pyroptosis (**Figure 5**) [22]. Since caspase-4 can restrict numerous other
258 Gram-negative bacteria [62, 64], and the pathogen *Shigella* inhibits the caspase-4 inflammasome
259 by multiple mechanisms to survive [65-67], and corneal epithelial cells were shown to express
260 caspase-4 [54], we tested the hypothesis that caspase-4 was involved in driving cell death in
261 response to intracellular *P. aeruginosa*. We generated *CASP4* knockout corneal epithelial cells
262 using CRISPR-Cas9, and loss of caspase-4 protein was confirmed by Western blot (**Supplemental**
263 **Figure 2**). Control cell lines with non-targeting guide RNA were also generated using an identical
264 selection strategy and grown up as monoclonal lines; each exhibited death rates consistent with
265 wild type, non-transduced hTCEpi cells (**Supplemental Figure 3**).
266
267 Invasion by wild type PAO1 yielded similar cell death timing in both *CASP4* knockout cells as
268 wild type corneal epithelial cells (**Figure 6A, B**). In contrast, Δ*exoSTY* mutant-invaded cells
269 experienced significantly increased cell survival times, which subsequently allowed substantial
270 further accumulation of intracellular bacteria (**Figure 6A, C**). A smaller but significant increase
271 of invaded cell survival times were also observed with PAO1Δ*exsA* mutant-occupied *CASP4*
272 knockout cells (**Figure 6D**). These data implicated the non-canonical inflammasome as a
273 dominant response to cytoplasmic invasion of T3SS-positive *P. aeruginosa* independently of the
274 T3SS effectors, and also show involvement in responding to vacuole-occupying *P. aeruginosa*
275 that do not express the T3SS. This finding that cell death rates for wild-type PAO1 remain
276 unchanged in *CASP4* knockout cells aligns with our previously published data showing that the
277 T3SS effector exotoxins, specifically the ADP ribosyltransferase activity of ExoS [19], counters
278 cell death. Of note, while *CASP4* knockout reduced corneal epithelial cell death associated with

279 intracellular Δ*exsA* mutants, many of the cells still died by the end of the 20-hour imaging time
280 frame (**Figures 1 and 6D**). This suggests additional mechanisms for recognizing vacuolar/T3SS-
281 negative *P. aeruginosa* in addition to caspase-4, and that they are also absent from HeLa cells.
282
283 **IFN-γ-stimulation enables HeLa cells to respond to intracellular *P. aeruginosa*.** HeLa cells
284 can support cytoplasmic hyper-replication of *P. aeruginosa* before significant impact on host cell
285 viability occurs [3, 19]. The bacterium *Salmonella* accomplishes a similar feat [68]. However,
286 Santos and colleagues demonstrated that IFN-γ stimulation causes HeLa cells to lyse in response
287 to *Salmonella* entry into the cytosol, which was associated with upregulation of GBP proteins and
288 stimulation of the caspase-4 inflammasome. [62]. Here, we examined the impact of IFN-γ
289 stimulation on the HeLa cell response to intracellular *P. aeruginosa*. HeLa cells were treated with
290 50 ng/ml IFN-γ for 16 hours prior to infection and compared to untreated cells (**Figure 7**). The
291 kinetics of wild type PAO1-induced host cell death remained unchanged. However, the rate of cell
292 death increased for both PAO1Δ*exoSTY* and for PAO1Δ*exsA* infections (**Figure 1 and 7**). [60];
293 IFN-γ-treated HeLa cells occupied by Δ*exsA* mutants died over varied timepoints during the 20
294 hours of infection similar to results for corneal epithelial cells. Aligning with the quick timing of
295 cell lysis, PAO1Δ*exoSTY* mutants were no longer able to replicate effectively in the cytoplasm of
296 IFN-γ-treated HeLa cells. Thus, IFN-γ-treated HeLa cells resembled corneal epithelial cells in their
297 response to intracellular *P. aeruginosa*. This suggests that the difference between corneal epithelial
298 cells and HeLa cells observed here may be among interferon stimulated genes (such as GBP1-4 in
299 unstimulated cells), or the ability of corneal epithelial cells to promptly upregulate components of
300 the caspase-4 pathway in response to detection of extracellular *P. aeruginosa*, prior to invasion
301 (**Figure 4**).

302

303 **Discussion**

304

305 Invasive (ExoS-expressing) strains of *P. aeruginosa* can thrive inside a wide range of host cells
306 [2, 3, 5]. After invasion of an epithelial cell, ExoS plays multiple roles in supporting intracellular
307 survival and replication, including inhibition of the host cell death response [19]. Here, we aimed
308 to understand the underlying cell death response inhibited by ExoS.

309

310 *P. aeruginosa* is highly adaptable and can adopt diverse phenotypes even in the same
311 environment. Previously, we used corneal and bronchial epithelial cells to show that after
312 invasion, members of the T3SS-positive population escape vacuoles to colonize the cytoplasm
313 while T3SS-off subpopulation members remain in vacuoles [59]. Because vacuoles containing
314 T3SS-off *P. aeruginosa* can become acidified, we originally assumed they were destined for
315 degradation in lysosomes [18]. However, we recently reported that vacuole-bound/T3SS-off
316 populations can report gene expression, including biofilm-associated genes, display enhanced
317 antibiotic resistance, and contribute to triggering host cell death [59]. These characteristics were
318 attributable to absence of the T3SS, with mutants lacking the T3SS (Δ*exsA* mutants) faithfully
319 replicating the phenotype.

320

321 Knowing *P. aeruginosa* diversifies intracellularly into vacuole- and cytoplasm- occupying
322 populations differing transcriptionally, that bacteria in both locations trigger cell death, that their
323 locations are determined by T3SS expression state, and that triggered host cell death can be
324 suppressed by the T3SS effector (ExoS), we used T3SS mutants trafficking to different locations

325 to interrogate mechanisms. Results using corneal epithelial cells showed that the death response
326 to intracellular *P. aeruginosa* lacking T3SS effectors (but expressing the T3SS apparatus)
327 involved caspase-4, its deletion inhibiting the rapid pyroptotic lysis. It also partially reduced
328 slower cell death caused by bacteria lacking the entire T3SS that were restricted to vacuoles
329 (Δ*exsA* mutants). We further found that while HeLa cells naturally lack this host cell death
330 response to intracellular *P. aeruginosa*, it could be induced by IFN-γ, a stimulator of numerous
331 genes including factors to assist in activation of the caspase-4 inflammasome [62]. Given that
332 ExoS expressed by wild-type *P. aeruginosa* inhibits the cell death response to intracellular
333 bacteria, these findings implicate ExoS-mediated interference with the non-canonical
334 inflammasome pathway/pyroptosis.
335
336 Since *P. aeruginosa* is often assumed an extracellular pathogen, previous studies of triggers or
337 manipulation of host epithelial cell death have been from the perspective of extracellular
338 bacteria. In that regard, ExoS has pro-cytotoxic activities. HeLa cells can undergo apoptotic cell
339 death based on both caspase-3 [60] and caspase-8 activity [69], and activation of apoptosis
340 through JNK1 and cytochrome c release [70]. This was also shown using a mammalian
341 expression system for introducing ExoS in the absence of bacteria, which showed it was
342 sufficient to induce HeLa cell apoptosis even in the absence of bacterial interaction [71]. Placing
343 our findings into the context of these earlier HeLa cell studies, we note differences in our
344 experimental systems: while they explored mechanisms for cell death caused by ExoS, we
345 studied cell death triggered by live bacteria inside cells when they lack ExoS. Were intracellular
346 bacteria present in these assays, the HeLa cells used would not have responded to them without
347 stimulation. Our experiments also provide an analysis of only invaded cells excluding

348 extracellular bacteria to focus on impact of intracellular bacteria, and used corneal cells which
349 naturally respond to them. We then showed that IFN-γ-stimulated HeLa cells respond in the
350 same manner: ExoS inhibits rather than drives a host cell death response. In sum, while
351 introducing ExoS in isolation is a useful surrogate for *in vitro* experimentation to address specific
352 questions, other bacterial factors/live bacteria can modify impact in other situations. Our data
353 also highlight the value of using cell lines that have not been substantially transformed, and
354 imaging studies to put into perspective important information resulting from biochemical
355 analyses. Despite differences in experimental models, it remains important to reconcile
356 outcomes, and the innate ability of ExoS to both drive and inhibit cell death, involving different
357 types of regulated cell death, and correlating with presence or absence of internalized *P.*
358 *aeruginosa,* is interesting and worth exploring. Indeed, it could aid in determining mechanisms
359 by which ExoS blocks pyroptosis, given crosstalk between pyroptosis and apoptosis noted in
360 other cell types [72].
361
362 While HeLa cells are reported to express caspase-4, results presented in this report showed that
363 activation in this context requires upregulation of IFN-γ stimulated genes, which include GBP
364 proteins that can bind and assist in presenting LPS [62]. It remains unknown if GBP proteins are
365 present or efficiently upregulated in corneal epithelial cells upon exposure to *P. aeruginosa*,
366 however detection of LPS is how other Gram-negative intracellular bacteria such as *Shigella*
367 trigger caspase-4. While our results with Δ*exsA* mutants raises questions about how LPS is
368 detected by factors in the cytoplasm when bacteria remain in vacuoles, proposed mechanisms in
369 other studies include outer membrane vesicle delivery [73] or by HMGB1 [74]. Our findings in

370 this regard are consistent with the observations of others who showed caspase-11 or caspase-5
371 activation in response to *P. aeruginosa*. [56, 75].
372
373 Interaction of GBP proteins (specifically, GBP2) with *P. aeruginosa* for efficient caspase-11
374 activation has been shown by Balakrishnan et. al*,* interestingly, in the context of T3SS-negative
375 cytotoxic bacteria (ExoU-producing) that are internalized by macrophages [75]. Usually, ExoU
376 encoding strains do not invade cells because T3SS injection from outside the cell causes rapid
377 cell death [76]. Although wild type *P. aeruginosa* is not known to replicate inside macrophages
378 in the same manner as in epithelial cells [7], the authors found that elimination of caspase-11 in
379 mouse BMDMs permitted intracellular proliferation of PopB mutants [75]. Despite differences
380 between the study by Balakrishnan et. al. and our experimental system, the importance of
381 caspase-4/11 in restricting intracellular *P. aeruginosa* niches is consistent. This supports the
382 possibility that ExoS could sustain intracellular niches by targeting these pathways in a broad
383 range of cell types and infection sites.
384
385 The specific mechanism by which the ADP-r activity of ExoS interferes with caspase-4-mediated
386 host cell lysis remains to be determined. Recently, *Shigella flexneri* was shown to block the non-
387 canonical inflammasome by two separate mechanisms: caspase-4 inactivation by a newly-
388 identified catalytic activity termed ADP-riboxanation by the effector OspC3 [65, 66], and
389 ubiquitylating gasdermin D with IpaH7.8 to target it for degradation [77]. ExoS is unique among
390 bacterial ADP ribosyltransferases for having numerous host substrates, and currently none have
391 been shown to interact specifically with the caspase-4/11 pathway [78]. Since there are many
392 possibilities to investigate, comprehensive identification of uncharacterized ExoS substrates and

393 their potential involvement will require a separate study. Considering the T3SS apparatus of
394 extracellular *P. aeruginosa* can trigger cell death via NLRC4 [79], and that *CASP4* knockout
395 does not fully prevent the cell death triggered by vacuole-bound T3SS mutants (**Figure 6**), it
396 would also be worth exploring if additional cell death pathways are impacted by ExoS.
397
398 In summary, the results of this study demonstrate a role for caspase-4 in limiting intracellular
399 colonization by *P. aeruginosa*, a phenomenon triggered by the presence of intracellular bacteria
400 but inhibited by the T3SS effector ExoS. Together with research previously published by us and
401 others using corneal, bronchial, and stimulated HeLa cells, this suggests the following sequence
402 of events for the intracellular lifestyle of invasive *P. aeruginosa:* bistable T3SS expression upon
403 host cell contact, invasion of T3SS-negative bacteria, cytoplasmic access associated with
404 intracellular T3SS activation, triggering of caspase-4 mediated pyroptosis, and inhibition of both
405 pyroptosis and autophagy by ExoS.
406
407 While providing more information about *P. aeruginosa*-host epithelial cell interactions, the data
408 presented in this report illustrate the value of quantitative imaging in teasing apart complexities
409 for a pathogen as versatile as *P. aeruginosa*. They also highlight the importance of appreciating
410 differences between cell types, including results showing a relevant mechanism lacking in a cell
411 line can remain a useful experimental system with host response factors that can be toggled on
412 and off using alternate means of stimulation (IFN-γ, in this instance). Importantly, the data
413 continue to support the notion that *P. aeruginosa* can function as both an intracellular and
414 extracellular pathogen, suggestive of a T3SS effector function devoted to inhibition of an
415 *intracellular* pattern recognition receptor, consistent with its unusual capacity to adapt to its

416 environment, survive hardship, and exist ubiquitously. Ultimately, development of effective
417 strategies to prevent or treat the devastating infections caused by *P. aeruginosa* will require a
418 thorough appreciation of these complexities.
419
420 **Methods**
421 **Bacterial strains, cell lines, and reagents.** *P. aeruginosa* strain PAO1 (a strain with positive
422 T3SS expression) and isogenic deletions of *exsA*, or ExoS/ExoT/ExoY were used for all
423 infection experiments [80]. Bacteria were grown at 37°C on tryptic soy agar. Plasmids used for
424 visualization were pJNE05 [81] and pBAD-GFP [59]. Plasmid selection was achieved with 100
425 µg/ml gentamicin. Corneal epithelial cells (hTCEpi) [55] were maintained in complete KGM-2
426 media (Lonza), lacking gentamicin. All experiments were conducted on cells between passage 49
427 and 70. HeLa cells were maintained in phenol red-free DMEM (Gibco) with 10% FBS.
428
429 **CRISPR-Cas9 knockout cell lines.** Lentiviral particles for transduction were generated from
430 293T cells transfected with psPAX2 (Didier Trono, Addgene plasmid # 12260 ;
431 http://n2t.net/addgene:12260 ; RRID:Addgene_12260) and pMD.2 (Didier Trono, Addgene
432 plasmid # 12259 ; http://n2t.net/addgene:12259 ; RRID:Addgene_12259), combined with either
433 Cas9 expression vector plenti-Cas9-blast (Feng Zhang, Addgene plasmid # 52962 ;
434 http://n2t.net/addgene:52962 ; RRID:Addgene_52962) [82] or a guide RNA vector plenti-LIC-
435 Puro which was adapted for ligation-independent cloning (kindly gifted by Moritz Gaidt) [83].
436 Guide RNA sequences targeting caspase-4 (5'- CCACAGAAAAAAGCCACTTA - 3') or a non-
437 targeting control sequence (5'- GACGGAGGCTAAGCGTCGCA - 3') were cloned into plenti-
438 LIC-Puro using ligation independent cloning. Six hours after transfection, media on 293T cells

439 was replaced with KGM-2. Media was collected at 48 hours and passed through a 0.45 µm filter
440 and added directly to hTCEpi cells, which were then centrifuged at 1200g for 90 minutes at
441 37°C. Antibiotic selection with blasticidin (50 µg/ml) or puromycin (10 µg/ml) was performed
442 after two days. For generation of monoclonal lines, cells were lifted by trypsin and seeded as
443 single cells in 96-well plates. Isolated colonies were identified and grown up over approximately
444 12 days before transfer into 6-well plates to avoid differentiation induced by crowding or
445 confluence. *CASP4* knockout candidates were screened by Western blot: lysates from a 6-well
446 plate were collected in 150 µl RIPA buffer, frozen and thawed, and then clarified by
447 centrifugation for 20 minutes at 4ºC. Samples were run on 10% stain free gels (Bio-Rad) and
448 total protein visualized as a loading control prior to transfer to 0.2 µm PVDF membrane.
449 Membrane was blocked with Bio-Rad commercial block for 10 minutes, and probed with anti-
450 caspase-4 antibody (Santa Cruz, sc-56056, 1:1000 or 100 ng/ml) overnight at 4ºC with rocking.
451 Blot was washed using TBST, and antibody detected with goat-anti-rabbit HRP (Bio-Rad,
452 1706515, 1:5000).
453
454 **Infection experiments.** Corneal epithelial cells were plated on No. 1.5 glass bottom 24 well
455 plates (MatTek) in KGM-2 with 1.15mM total calcium induce differentiation [55]. Corneal cells
456 were plated at 75% confluence the day prior to experiments. HeLa cells were maintained in
457 DMEM with 10% FBS and plated at 50% confluence the day prior to experiments. For imaging,
458 HeLa cells were plated on optical plastic 8-well chambered coverslips (ibidi). Where indicated,
459 50 ng/ml IFN-γ (Peprotech) was added at 16 hours prior to infections of HeLa cells and
460 maintained throughout the infection and imaging.
461

462 Bacterial suspensions were made in PBS from 16-hour lawns grown on TSA media at 37°C. The
463 optical density at 540 nm was measured, and generally ranged from 1-4. An MOI of 10 was
464 calculated using OD540 of 1 equal to 4 x 10^8 CFU per mL. Bacteria (volumes typically 0.5-4 µl)
465 were directly added to cell culture media and allowed to infect for 3 hours. For live imaging
466 experiments, Hoechst (0.8 µg/ml) was added to the cells prior to infections and allowed to label
467 the cells during the 3-hour infection period. Then media was removed, and replaced with media
468 containing the antibiotic amikacin (200 µg/ml) and propidium iodide (0.75 µg/ml). Where
469 needed, a 1:10 dilution of 10% arabinose in either KGM-2 or DMEM was added at 3.75 hours
470 post infection, which induced GFP expression in the protected population of intracellular
471 bacteria carrying the pBAD-GFP plasmid.
472
473 **Bacterial killing.** Aliquots of bacterial inocula were measured by spectrophotometry and
474 volumes to be added to achieve effective MOIs of 10, 160, or 640 were determined as above.
475 Heat-killed bacteria were boiled for 10 minutes. Paraformaldehyde-killed bacteria were fixed in
476 a 2% solution of paraformaldehyde in PBS for 10 minutes, quenched with 150mM glycine for 10
477 minutes, and washed in PBS using centrifugation. Amikacin-killed bacteria were exposed to
478 1000 µg/ml amikacin for 30 minutes or 3 hours prior to adding to cells. All bacteria were plated
479 on TSA agar in 5 µl volumes to ensure complete killing.
480
481 **RT-PCR arrays.** Cells in 10cm dishes were infected with PAO1, PAO1Δ*exoSTY*, or
482 PAO1Δ*exsA* for 3 hours at an MOI of 10, and media was replaced for 1 hour with 200 µg/ml
483 amikacin. At 4 hours, cells were washed twice in PBS and collected in 1ml TriReagent (Sigma).
484 RNA was collected using Zymo Direct-zol RNA MiniPrep with in-column DNAse digestion for

485 an extended time of 40 minutes. RNA quality was assessed by BioAnalyzer at QB3 Genomics,
486 UC Berkeley, Berkeley, CA, RRID:SCR_022170. cDNA synthesis using 0.5µg of RNA was
487 performed with the RT2 first strand kit (Qiagen) according to manufacturer's instructions. The
488 RT² Profiler™ PCR Array Human Cell Death PathwayFinder (PAHS-212Z, Qiagen) product
489 was selected, and RT PCR performed on a Roche LightCycler 96 instrument. Analysis was
490 performed using Qiagen's Data Center Analysis Portal.
491 (https://geneglobe.qiagen.com/us/analyze). Graphs of results were prepared using Graph Pad
492 Prism 9.
493
494 **Fixed immunostaining.** Cells were seeded on No. 1.5 glass coverslips and infected as described
495 above. At four hours post infection, cells were washed twice in PBS and fixed in 4%
496 paraformaldehyde in PBS for 10 m. Cells were washed twice in PBS, and free aldehydes
497 neutralized with 150 mM glycine in PBS for 10 minutes. Then cells were washed twice in PBS,
498 and permeabilized and blocked (5% FBS, 2.5% cold fish skin gelatin, 0.1% TritonX-100, 0.05%
499 Tween-20 in PBS) for 1 hour. Then primary antibody was added in antibody solution (2.5%
500 FBS, 1.25% cold fish skin gelatin, 0.1% TritonX-100, 0.05% Tween-20 in PBS) overnight at
501 4°C. Cells were washed 4 times (5 minutes per wash), and secondary antibodies were added in
502 antibody solution for 1 hour in darkness. Cells were washed once, labeled with DAPI for 5 m,
503 and washed two more times (5 minutes each). Coverslips were mounted on ProLong Diamond
504 and cured overnight prior to imaging.
505
506 **Microscopy.** Images for Figs 1, 3, and 5 were captured on a Nikon Ti-E inverted microscope
507 equipped with a Lumencor Spectra X LED Light Engine illumination source. All other images

508 were captured on a Ti2-E inverted microscope base with X-Cite XYLIS XT720S Broad
509 Spectrum LED Illumination System. Both systems used Nikon perfect focus, an Okolab stage-
510 top incubation chamber, a DS-Qi2 CMOS camera, CFI Plan Apochromat Lambda D 40X air NA
511 0.95 objective for time lapse images, and CFI Plan Apochromat Lambda D 60X Oil NA 1.42
512 objective for fixed slides. For time lapses, fields were selected between hours 3 and 4 without
513 observation of fluorescence channels to avoid bias. Eight fields per condition were imaged
514 hourly from 4 to 20 hours post infection.
515
516 **Image Analysis.** Time-lapse images were computationally analyzed using two custom macros
517 written for the FIJI package of Image J, with final results table encoded as intensity values in a
518 TIF image, which was previously described [19]. The code for measuring rates of cell death for
519 the whole population, and set of macros for tracking the invasion state of cells is available in a
520 GitHub repository: https://github.com/Llamero/Nuclei_analysis-macro. Subsequent Python
521 scripts for exporting the analysis TIF file and processing it are available in the following GitHub
522 repository: https://github.com/abbykroken/cell_survival_with_bacteria.
523
524 **In vitro T3SS effector secretion.** Bacteria were grown for 5 hours in 5ml LB media
525 supplemented with 100mM MSG and 1% glycerol at 37ºC with shaking at 200 rpm. A
526 concentration of 2mM EGTA was added to induce T3 secretion. Final concentrations of 1% or
527 0.1% arabinose were added from a 10% stock made in LB media with MSG and glycerol. OD
528 540 nm readings were taken prior to supernatant protein concentration and used to normalize
529 sample volumes. Bacteria were centrifuged at 12000g to clarify 1ml of supernatant. Proteins
530 were concentrated using TCA precipitation: to 1ml of supernatant, 250 µl of 100% cold TCA

531 was added for 30 minutes, and then centrifuged at 14000g for 5 minutes. The pellet was washed
532 with 1ml of cold acetone twice, briefly dried, and suspended in 4x laemmli buffer based on the
533 starting OD (max volume of 50 µl). Proteins were visualized using 10% stain-free gels (Bio-
534 Rad).
535
536 **Statistics.** Statistical analyses were performed and data presented using Graph Pad Prism 9. Super
537 violin plots were prepared using scripts published by Kenny and Schoen [63] and output images
538 aligned on axes generated in Graph Pad Prism 9. Data were shown as a mean ± standard deviation
539 (SD) of 3-6 independent experiments unless otherwise indicated. Comparison of two groups was
540 performed by Student's t-test, three or more groups by One-way ANOVA with Tukey's post-hoc
541 analysis. Comparison between two groups for total cell death rates overtime was performed by
542 multiple column t-tests for each timepoint, and the two samples that were compared are specified
543 in the figure legends. In each instance, * $P < 0.05$, ** $P < 0.01$, *** $P < 0.005$ and **** $P < 0.001$.
544
545 **Acknowledgements**
546 Thanks to Arne Rietsch (Case Western Reserve University, OH) for providing *P. aeruginosa* wild-
547 type strains and mutants, Timothy L Yahr (University of Iowa, IA) for plasmid pJNE05, and
548 Danielle M Robertson (University of Texas Southwestern, TX) for providing the telomerase-
549 immortalized human corneal epithelial cells. Thanks to Benjamin E Smith (University of
550 California, Berkeley, CA) for continued support of FIJI image analysis macros. We also thank
551 Russell E Vance (University of California, Berkeley, CA) for helpful suggestions during the course
552 of this project.
553

554 ARK, PSM, VN, DJE, and SMJF designed the experiments; ARK, KAK, PSM, and EJJ performed
555 the experiments; ARK, KAK, PSM, VN, DJE, SMJF analyzed and interpreted the data; ARK,
556 DJE, and SMJF wrote the manuscript; ARK, DJE, and SMJF supervised the study.
557
558 This work was supported by the National Institutes of Health R01 EY011221 (SMJF),
559 R01EY034239 (ARK), F32 EY025969 (ARK), DP2 AI154432 (PSM), P30 DK089507 (PSM),
560 F32 EY029152 (VN), and the Mallinckrodt Foundation (PSM). The funding agencies had no role
561 in the study design, data collection and interpretation, or decision to submit the work for
562 publication.

563 **Figure 1. Host cell death rates from *P. aeruginosa* mutant infections**. **(A)** Corneal epithelial
564 cells (hTCEpi) were infected with indicated strain: wt PAO1, PAO1Δ*exoSTY*, or PAO1Δ*exsA* for
565 3 hours at an MOI equal to 10. Hoechst (blue) was added to label nuclei. Non-associated bacteria
566 were removed, and media with amikacin and propidium iodide (red) was added to kill extracellular
567 bacteria. Cells were imaged hourly from 4 to 20 hours post infection. Select fields from indicated
568 times are shown. **(B)** The percent of cells positive for propidium iodide at each timepoint was
569 determined by using a custom FIJI macro to segment all nuclei from the Hoechst channel, and all
570 nuclei of dead cells in the propidium iodide channel. Multiple column t-tests were performed
571 comparing wt PAO1 and PAO1Δ*exsA*, and SD error bars are displayed from three replicates. **(C)**
572 Experiment was performed identically as in panel A, but using HeLa cells. **(D)** Analysis was
573 performed as in panel B, using the data obtained in panel C.
574
575 **Figure 2. Live bacteria kill corneal epithelial cells.** Corneal epithelial cells (hTCEpi) were
576 infected with PAO1Δ*exsA* for 3 hours at an MOI of 10. An identical quantity of bacteria was boiled
577 for 10 minutes prior to infecting cells (**A**), fixed with 2% paraformaldehyde for 10 minutes before
578 infecting cells (**B**), or treated with 1000 µg/ml amikacin for 30 minutes before infecting cells (**C**).
579 MOIs of 160 and 640 were accomplished by adding a greater volume of the same inoculum, which
580 accounts for live bacterial replication from the initial MOI of 10 during the 3-hour infection period.
581 Hoechst (blue) was added to label nuclei. Non-associated bacteria were removed, and media with
582 amikacin and propidium iodide (red) was added. Cells were imaged hourly from 4 to 20 hours post
583 infection. Panels A-C were conducted simultaneously with different bacterial killing methods
584 displayed on separate graphs. (**D**) Experiment conducted as in panel C, however a subset of
585 PAO1Δ*exsA* bacteria were exposed to amikacin for either 30 minutes or 3 hours prior to

586 inoculation of corneal epithelial cells. Cell labeling and analysis was conducted identically to prior
587 panels. Each experiment was conducted twice, and a represented replicate is shown.
588
589 **Figure 3. Intracellular Δ*exsA* mutants kill invaded cells at a similar rate to wt PAO1-invaded**
590 **cells. (A)** Bacteria were transformed with an arabinose-inducible GFP plasmid. Corneal epithelial
591 cells (hTCEpi) were infected at an MOI of 10 and extracellular bacteria eliminated at 3 hours post
592 infection using amikacin. A final concentration of 1% arabinose was used to induce GFP in
593 surviving intracellular bacteria beginning at 3.5 hours post infection. Time lapse imaging was
594 conducted hourly from 4 to 20 hours, and host cell nuclei detected with Hoechst and propidium
595 iodide to determine time of death. Insets 1-2 show the boxed cell at 6 or 11 hours post infection,
596 respectively. **(B)** An example of a live invaded cell from 20 hours post infection. **(C)** Example of
597 a dead invaded cell from 20 hours post infection, where the PI channel has been saturated such
598 that PI-positive bacteria can be visualized. **(D)** The T3SS-GFP reporter pJNE05 was used to
599 visualize wt PAO1 and PAO1Δ*exoSTY* infections, as described previously [19], to compare to
600 PAO1Δ*exsA* infections. Time lapses from panels A through D are available as **Supplemental**
601 **Movie 2**. **(E)** A computational analysis approach was used to segregate only invaded cells, and
602 determine their survival time in hours. The survival times of all invaded cells from six replicates
603 were combined into a single super violin plot. Mean survival times with SD error bars are
604 displayed, and significance determined by One-way ANOVA. *** $P < 0.005$.
605
606 **Figure 4. Transcriptional responses of infected host cells. (A)** Corneal epithelial cells (hTCEpi)
607 were infected with wt PAO1, PAO1Δ*exoSTY*, or PAO1Δ*exsA* for 3 hours at an MOI equal to 10.
608 Non-associated bacteria were removed, and media with amikacin was added for 1 additional hour.

609 At four hours, RNA was purified from infected cells, and RT PCR analysis performed using a
610 commercial array for genes associated with specific cell death pathways. **(B)** Experiment
611 performed identically to panel A, except using HeLa cells.
612
613 **Figure 5. NF-κB signaling and the role of secreted factors in cell death. (A)** Corneal epithelial
614 cells (hTCEpi) were infected with wt PAO1, PAO1Δ*exoSTY*, or PAO1Δ*exsA* for 3 hours at an
615 MOI equal to 10. Then media was replaced with amikacin-containing media. Cells were fixed at
616 4 hours post infection and p65 localization was determined using immunofluorescent staining.
617 Nuclei were labeled with DAPI. **(B)** Experiment performed identically to panel A, using HeLa
618 cells. **(C)** Corneal epithelial cells were infected as described in panel A. Supernatant of infected
619 cells was collected at 4 hours post infection and TNFα measured by ELISA. **(D)** Supernatants of
620 corneal epithelial cells infected with PAO1Δ*exoSTY*, PAO1Δ*exsA*, or uninfected were collected at
621 4 hours post infection and sterilized with 0.22 μm filter, and used as the replacement media on
622 uninfected cells or PAO1Δ*exsA* infected cells at 3 hours post infection, combined with amikacin
623 and propidium iodide. Hoechst was used to label all nuclei. The cell death rates were measured by
624 time lapse imaging, error bars display SD from three replicates.
625
626
627 **Figure 6. Caspase-4 limits intracellular replication and persistence of T3SS mutant bacteria.**
628 (A) Corneal epithelial cells (hTCEpi) or cells knocked out for caspase-4 were infected with wt
629 PAO1, PAO1Δ*exoSTY* (each visualized by T3SS-GFP reporter) or PAO1Δ*exsA* (pBAD-GFP
630 induced) at an MOI of 10. Nuclei were labeled with Hoechst and Propidium iodide. Extracellular
631 bacteria were eliminated with amikacin at 3 hours post infection, and imaged hourly from 4 to 20

632 hours post infection. Images from 8 hours post infection are shown. Full-field time lapses are
633 available as **Supplemental Movie 3**. (**B-D**) Cells from wt PAO1 (B), PAO1Δ*exoSTY* (C), or
634 PAO1Δ*exsA* (D) infections were analyzed with a computational approach to segregate only
635 invaded cells and measure survival times in hours. Six replicates were combined into a single super
636 violin plot. Mean survival times with SD error bars are displayed, and significance determined by
637 Student's t-test.
638
639 **Figure 7. IFN-γ-stimulated HeLa cells are not permissive for PAO1Δ*exoSTY* intracellular**
640 **replication nor PAO1Δ*exsA* intracellular persistence. (A)** HeLa cells were treated with 50
641 ng/ml IFN-γ for 16 hours prior to infection with wt PAO1, PAO1Δ*exoSTY* (each using the T3SS-
642 GFP reporter) or PAO1Δ*exsA* (pBAD-GFP induced) at an MOI of 10. Nuclei were labeled with
643 Hoechst and Propidium iodide. Extracellular bacteria were eliminated with amikacin at 3 hours
644 post infection, and imaged hourly from 4 to 20 hours post infection. Select time frames are shown
645 at either 10 or 15 hours post infection. Full-field time lapses are available as **Supplemental Movie**
646 **4**. **(B)** The rate of cell death was determined using host cell nuclear stains. All panels are from the
647 same experiment with only indicated bacterial strain shown. Error bars show SD from three
648 replicates. Multiple column t-tests were performed comparing IFN-γ-treated cells to untreated.
649
650 **Supplemental Figure 1. GFP expression from plasmid pBAD-GFP suppresses the T3SS.** (A)
651 wt PAO1 was transformed with the T3SS reporter plasmid pJNE05, or the GFP inducible plasmid
652 pBAD-GFP and imaged hourly in time lapse. Example fields are shown in which bacteria
653 expressing GFP under the T3SS reporter exhibit intracellular spread and replication, whereas those
654 with inducible GFP show only limited intracellular replication. (B) The cell death rates of wt PAO1

655 or PAO1Δ*exoSTY* expressing GFP by either plasmid were measured, showing a trend of reduced
656 cell killing rates for PAO1Δ*exoSTY* when GFP expression is induced. (C) wt PAO1 with indicated
657 plasmid was grown for 5 hours in LB media with EGTA to induce the T3SS, and arabinose to
658 induce GFP. Supernatant proteins were concentrated by TCA precipitation, and the bands
659 constituting ExoS and ExoT are indicated.
660
661 **Supplemental Figure 2. Confirmation of caspase-4 deletion.** Lysates from wt hTCEpi cells or
662 caspase-4 candidate knockout cells were collected in RIPA buffer and clarified. Total protein was
663 visualized using Bio-Rad stain free gels prior to transfer. Blot was probed with anti-caspase-4
664 antibody.
665
666 **Supplemental Figure 3. Control monoclonal cells for CRISPR-Cas9 mutagenesis.** A control
667 cell line was generated using non-targeting guide RNA, and monoclonal line generated. Cells were
668 infected with wt PAO1, PAO1Δ*exoSTY* (each using the T3SS-GFP reporter) or PAO1Δ*exsA*
669 (pBAD-GFP induced) at an MOI of 10. Nuclei were labeled with Hoechst and Propidium iodide.
670 Extracellular bacteria were eliminated with amikacin at 3 hours post infection, and imaged hourly
671 from 4 to 20 hours post infection. Images were analyzed with a computational approach to
672 segregate invaded cells and measure survival times in hours. Three replicates were combined into
673 a single super violin plot. Mean survival times with SD error bars are displayed.
674
675 **Supplemental Movie 1. Amikacin-killed bacteria retain motility.** Corneal epithelial cells were
676 inoculated with amikacin-killed (1000 µg/ml for 30 minutes) or paraformaldehyde-killed (2% for
677 10 minutes) PAO1Δ*exsA* bacteria and immediately observed using differential interference

678 contrast imaging, captured in real time.

679

680 **Supplemental Movie 2. Corneal epithelial cells invaded by *P. aeruginosa* and mutants.**
681 Corneal epithelial cells (hTCEpi) were infected with wt PAO1, PAO1Δ*exoSTY* (each expressing
682 GFP by T3SS reporter), or PAO1Δ*exsA* (inducible GFP) for 3 hours at an MOI equal to 10. Then
683 media was replaced with amikacin-containing media. Arabinose was added to PAO1Δ*exsA*
684 condition at 3.5 hours post infection. Imaging was conducted hourly from 4 to 20 hours.

685

686 **Supplemental Movie 3. *CASP4* knockout corneal epithelial cells invaded by *P. aeruginosa***
687 **and mutants.** Corneal epithelial cells (hTCEpi) or *CASP4* knockout cells were infected with wt
688 PAO1, PAO1Δ*exoSTY* (each expressing GFP by T3SS reporter), or PAO1Δ*exsA* (inducible GFP)
689 for 3 hours at an MOI equal to 10. Then media was replaced with amikacin-containing media.
690 Arabinose was added to PAO1Δ*exsA* condition at 3.5 hours post infection. Imaging was conducted
691 hourly from 4 to 20 hours.

692

693 **Supplemental Movie 4. IFN-γ-stimulated HeLa cells invaded by *P. aeruginosa* and mutants.**
694 HeLa cells were treated with 50 ng/ml IFN-γ for 16 hours prior to infection with wt PAO1,
695 PAO1Δ*exoSTY* (each using the T3SS-GFP reporter) or PAO1Δ*exsA* (pBAD-GFP induced) at an
696 MOI of 10. Nuclei were labeled with Hoechst and Propidium iodide. Extracellular bacteria were
697 eliminated with amikacin at 3 hours post infection, and imaged hourly from 4 to 20 hours post
698 infection. Arabinose was added to PAO1Δ*exsA* condition at 3.5 hours post infection. Imaging was
699 conducted hourly from 4 to 20 hours. IFN-γ was maintained during infection and imaging.

700 **References**
701

702 1. Angus AA, Lee AA, Augustin DK, Lee EJ, Evans DJ, Fleiszig SM. Pseudomonas aeruginosa
703 induces membrane blebs in epithelial cells, which are utilized as a niche for intracellular replication and
704 motility. Infect Immun. 2008;76(5):1992-2001. Epub 2008/03/05. doi: 10.1128/IAI.01221-07. PubMed
705 PMID: 18316391; PubMed Central PMCID: PMCPMC2346716.
706 2. Jolly AL, Takawira D, Oke OO, Whiteside SA, Chang SW, Wen ER, et al. Pseudomonas
707 aeruginosa-induced bleb-niche formation in epithelial cells is independent of actinomyosin contraction
708 and enhanced by loss of cystic fibrosis transmembrane-conductance regulator osmoregulatory function.
709 mBio. 2015;6(2):e02533. Epub 2015/02/26. doi: 10.1128/mBio.02533-14. PubMed PMID: 25714715;
710 PubMed Central PMCID: PMCPMC4358002.
711 3. Kroken AR, Chen CK, Evans DJ, Yahr TL, Fleiszig SMJ. The Impact of ExoS on Pseudomonas
712 aeruginosa Internalization by Epithelial Cells Is Independent of fleQ and Correlates with Bistability of
713 Type Three Secretion System Gene Expression. mBio. 2018;9(3). Epub 2018/05/03. doi:
714 10.1128/mBio.00668-18. PubMed PMID: 29717012; PubMed Central PMCID: PMCPMC5930308.
715 4. Fleiszig SM, Zaidi TS, Fletcher EL, Preston MJ, Pier GB. Pseudomonas aeruginosa invades
716 corneal epithelial cells during experimental infection. Infect Immun. 1994;62(8):3485-93. Epub
717 1994/08/01. doi: 10.1128/iai.62.8.3485-3493.1994. PubMed PMID: 8039920; PubMed Central PMCID:
718 PMCPMC302982.
719 5. Angus AA, Evans DJ, Barbieri JT, Fleiszig SM. The ADP-ribosylation domain of Pseudomonas
720 aeruginosa ExoS is required for membrane bleb niche formation and bacterial survival within epithelial
721 cells. Infect Immun. 2010;78(11):4500-10. Epub 2010/08/25. doi: 10.1128/IAI.00417-10. PubMed PMID:
722 20732998; PubMed Central PMCID: PMCPMC2976358.
723 6. Sana TG, Baumann C, Merdes A, Soscia C, Rattei T, Hachani A, et al. Internalization of
724 Pseudomonas aeruginosa Strain PAO1 into Epithelial Cells Is Promoted by Interaction of a T6SS Effector
725 with the Microtubule Network. mBio. 2015;6(3):e00712. Epub 2015/06/04. doi: 10.1128/mBio.00712-15.
726 PubMed PMID: 26037124; PubMed Central PMCID: PMCPMC4453011.
727 7. Garai P, Berry L, Moussouni M, Bleves S, Blanc-Potard AB. Killing from the inside: Intracellular
728 role of T3SS in the fate of Pseudomonas aeruginosa within macrophages revealed by mgtC and oprF
729 mutants. PLoS Pathog. 2019;15(6):e1007812. Epub 2019/06/21. doi: 10.1371/journal.ppat.1007812.
730 PubMed PMID: 31220187; PubMed Central PMCID: PMCPMC6586356.
731 8. Fleiszig SM, Zaidi TS, Preston MJ, Grout M, Evans DJ, Pier GB. Relationship between
732 cytotoxicity and corneal epithelial cell invasion by clinical isolates of Pseudomonas aeruginosa. Infect
733 Immun. 1996;64(6):2288-94. Epub 1996/06/01. doi: 10.1128/iai.64.6.2288-2294.1996. PubMed PMID:
734 8675339; PubMed Central PMCID: PMCPMC174068.
735 9. Coburn J, Dillon ST, Iglewski BH, Gill DM. Exoenzyme S of Pseudomonas aeruginosa ADP-
736 ribosylates the intermediate filament protein vimentin. Infect Immun. 1989;57(3):996-8. Epub
737 1989/03/01. doi: 10.1128/iai.57.3.996-998.1989. PubMed PMID: 2492977; PubMed Central PMCID:
738 PMCPMC313212.
739 10. Riese MJ, Goehring UM, Ehrmantraut ME, Moss J, Barbieri JT, Aktories K, et al. Auto-ADP-
740 ribosylation of Pseudomonas aeruginosa ExoS. J Biol Chem. 2002;277(14):12082-8. Epub 2002/02/01.
741 doi: 10.1074/jbc.M109039200. PubMed PMID: 11821389.
742 11. Goehring UM, Schmidt G, Pederson KJ, Aktories K, Barbieri JT. The N-terminal domain of
743 Pseudomonas aeruginosa exoenzyme S is a GTPase-activating protein for Rho GTPases. J Biol Chem.
744 1999;274(51):36369-72. Epub 1999/12/14. doi: 10.1074/jbc.274.51.36369. PubMed PMID: 10593930.
745 12. Iglewski BH, Sadoff J, Bjorn MJ, Maxwell ES. Pseudomonas aeruginosa exoenzyme S: an
746 adenosine diphosphate ribosyltransferase distinct from toxin A. Proc Natl Acad Sci U S A.
747 1978;75(7):3211-5. Epub 1978/07/01. doi: 10.1073/pnas.75.7.3211. PubMed PMID: 210453; PubMed
748 Central PMCID: PMCPMC392744.
749 13. McGuffie EM, Frank DW, Vincent TS, Olson JC. Modification of Ras in eukaryotic cells by
750 Pseudomonas aeruginosa exoenzyme S. Infect Immun. 1998;66(6):2607-13. Epub 1998/05/29. doi:

751 10.1128/IAI.66.6.2607-2613.1998. PubMed PMID: 9596723; PubMed Central PMCID:
752 PMCPMC108245.
753 14. Simon NC, Barbieri JT. Exoenzyme S ADP-ribosylates Rab5 effector sites to uncouple
754 intracellular trafficking. Infect Immun. 2014;82(1):21-8. Epub 2013/10/09. doi: 10.1128/IAI.01059-13.
755 PubMed PMID: 24101692; PubMed Central PMCID: PMCPMC3911848.
756 15. Maresso AW, Deng Q, Pereckas MS, Wakim BT, Barbieri JT. Pseudomonas aeruginosa ExoS
757 ADP-ribosyltransferase inhibits ERM phosphorylation. Cell Microbiol. 2007;9(1):97-105. Epub
758 2006/08/08. doi: 10.1111/j.1462-5822.2006.00770.x. PubMed PMID: 16889625.
759 16. Deng Q, Barbieri JT. Modulation of host cell endocytosis by the type III cytotoxin, Pseudomonas
760 ExoS. Traffic. 2008;9(11):1948-57. Epub 2008/09/10. doi: 10.1111/j.1600-0854.2008.00808.x. PubMed
761 PMID: 18778330; PubMed Central PMCID: PMCPMC2574883.
762 17. Rao L, De La Rosa I, Xu Y, Sha Y, Bhattacharya A, Holtzman MJ, et al. Pseudomonas
763 aeruginosa survives in epithelia by ExoS-mediated inhibition of autophagy and mTOR. EMBO Rep.
764 2021;22(2):e50613. Epub 2020/12/22. doi: 10.15252/embr.202050613. PubMed PMID: 33345425;
765 PubMed Central PMCID: PMCPMC7857434.
766 18. Heimer SR, Evans DJ, Stern ME, Barbieri JT, Yahr T, Fleiszig SM. Pseudomonas aeruginosa
767 utilizes the type III secreted toxin ExoS to avoid acidified compartments within epithelial cells. PLoS
768 One. 2013;8(9):e73111. Epub 2013/09/24. doi: 10.1371/journal.pone.0073111. PubMed PMID:
769 24058462; PubMed Central PMCID: PMCPMC3776860.
770 19. Kroken AR, Gajenthra Kumar N, Yahr TL, Smith BE, Nieto V, Horneman H, et al. Exotoxin S
771 secreted by internalized Pseudomonas aeruginosa delays lytic host cell death. PLoS Pathog.
772 2022;18(2):e1010306. Epub 20220207. doi: 10.1371/journal.ppat.1010306. PubMed PMID: 35130333;
773 PubMed Central PMCID: PMCPMC8853526.
774 20. Jorgensen I, Miao EA. Pyroptotic cell death defends against intracellular pathogens. Immunol
775 Rev. 2015;265(1):130-42. doi: 10.1111/imr.12287. PubMed PMID: 25879289; PubMed Central PMCID:
776 PMCPMC4400865.
777 21. Ulland TK, Ferguson PJ, Sutterwala FS. Evasion of inflammasome activation by microbial
778 pathogens. J Clin Invest. 2015;125(2):469-77. Epub 20150202. doi: 10.1172/JCI75254. PubMed PMID:
779 25642707; PubMed Central PMCID: PMCPMC4319426.
780 22. Galluzzi L, Vitale I, Aaronson SA, Abrams JM, Adam D, Agostinis P, et al. Molecular
781 mechanisms of cell death: recommendations of the Nomenclature Committee on Cell Death 2018. Cell
782 Death Differ. 2018;25(3):486-541. Epub 2018/01/25. doi: 10.1038/s41418-017-0012-4. PubMed PMID:
783 29362479; PubMed Central PMCID: PMCPMC5864239.
784 23. Cunha LD, Zamboni DS. Subversion of inflammasome activation and pyroptosis by pathogenic
785 bacteria. Front Cell Infect Microbiol. 2013;3:76. Epub 2013/12/11. doi: 10.3389/fcimb.2013.00076.
786 PubMed PMID: 24324933; PubMed Central PMCID: PMCPMC3840304.
787 24. Rayamajhi M, Zak DE, Chavarria-Smith J, Vance RE, Miao EA. Cutting edge: Mouse NAIP1
788 detects the type III secretion system needle protein. J Immunol. 2013;191(8):3986-9. Epub 20130916.
789 doi: 10.4049/jimmunol.1301549. PubMed PMID: 24043898; PubMed Central PMCID:
790 PMCPMC3819181.
791 25. Unterholzner L, Keating SE, Baran M, Horan KA, Jensen SB, Sharma S, et al. IFI16 is an innate
792 immune sensor for intracellular DNA. Nat Immunol. 2010;11(11):997-1004. Epub 20101003. doi:
793 10.1038/ni.1932. PubMed PMID: 20890285; PubMed Central PMCID: PMCPMC3142795.
794 26. Shi J, Zhao Y, Wang Y, Gao W, Ding J, Li P, et al. Inflammatory caspases are innate immune
795 receptors for intracellular LPS. Nature. 2014;514(7521):187-92. Epub 2014/08/15. doi:
796 10.1038/nature13683. PubMed PMID: 25119034.
797 27. Martinon F, Agostini L, Meylan E, Tschopp J. Identification of bacterial muramyl dipeptide as
798 activator of the NALP3/cryopyrin inflammasome. Curr Biol. 2004;14(21):1929-34. doi:
799 10.1016/j.cub.2004.10.027. PubMed PMID: 15530394.
800 28. Sandstrom A, Mitchell PS, Goers L, Mu EW, Lesser CF, Vance RE. Functional degradation: A
801 mechanism of NLRP1 inflammasome activation by diverse pathogen enzymes. Science. 2019;364(6435).

802 Epub 2019/03/16. doi: 10.1126/science.aau1330. PubMed PMID: 30872533; PubMed Central PMCID:
803 PMCPMC6532986.
804 29. Xu H, Yang J, Gao W, Li L, Li P, Zhang L, et al. Innate immune sensing of bacterial
805 modifications of Rho GTPases by the Pyrin inflammasome. Nature. 2014;513(7517):237-41. Epub
806 2014/06/12. doi: 10.1038/nature13449. PubMed PMID: 24919149.
807 30. Poyet JL, Srinivasula SM, Tnani M, Razmara M, Fernandes-Alnemri T, Alnemri ES.
808 Identification of Ipaf, a human caspase-1-activating protein related to Apaf-1. J Biol Chem.
809 2001;276(30):28309-13. Epub 20010604. doi: 10.1074/jbc.C100250200. PubMed PMID: 11390368.
810 31. Martinon F, Burns K, Tschopp J. The inflammasome: a molecular platform triggering activation
811 of inflammatory caspases and processing of proIL-beta. Molecular Cell. 2002;10(2):417-26. doi:
812 10.1016/s1097-2765(02)00599-3.
813 32. Kayagaki N, Warming S, Lamkanfi M, Vande Walle L, Louie S, Dong J, et al. Non-canonical
814 inflammasome activation targets caspase-11. Nature. 2011;479(7371):117-21. Epub 20111016. doi:
815 10.1038/nature10558. PubMed PMID: 22002608.
816 33. Vigano E, Diamond CE, Spreafico R, Balachander A, Sobota RM, Mortellaro A. Human caspase-
817 4 and caspase-5 regulate the one-step non-canonical inflammasome activation in monocytes. Nat
818 Commun. 2015;6:8761. Epub 20151028. doi: 10.1038/ncomms9761. PubMed PMID: 26508369; PubMed
819 Central PMCID: PMCPMC4640152.
820 34. Downs KP, Nguyen H, Dorfleutner A, Stehlik C. An overview of the non-canonical
821 inflammasome. Mol Aspects Med. 2020;76:100924. Epub 20201111. doi: 10.1016/j.mam.2020.100924.
822 PubMed PMID: 33187725; PubMed Central PMCID: PMCPMC7808250.
823 35. He WT, Wan H, Hu L, Chen P, Wang X, Huang Z, et al. Gasdermin D is an executor of
824 pyroptosis and required for interleukin-1beta secretion. Cell Res. 2015;25(12):1285-98. Epub 2015/11/28.
825 doi: 10.1038/cr.2015.139. PubMed PMID: 26611636; PubMed Central PMCID: PMCPMC4670995.
826 36. Kayagaki N, Stowe IB, Lee BL, O'Rourke K, Anderson K, Warming S, et al. Caspase-11 cleaves
827 gasdermin D for non-canonical inflammasome signalling. Nature. 2015;526(7575):666-71. Epub
828 2015/09/17. doi: 10.1038/nature15541. PubMed PMID: 26375259.
829 37. Ding J, Wang K, Liu W, She Y, Sun Q, Shi J, et al. Pore-forming activity and structural
830 autoinhibition of the gasdermin family. Nature. 2016;535(7610):111-6. Epub 20160608. doi:
831 10.1038/nature18590. PubMed PMID: 27281216.
832 38. Karmakar M, Minns M, Greenberg EN, Diaz-Aponte J, Pestonjamasp K, Johnson JL, et al. N-
833 GSDMD trafficking to neutrophil organelles facilitates IL-1beta release independently of plasma
834 membrane pores and pyroptosis. Nat Commun. 2020;11(1):2212. Epub 2020/05/07. doi: 10.1038/s41467-
835 020-16043-9. PubMed PMID: 32371889; PubMed Central PMCID: PMCPMC7200749.
836 39. DiPeso L, Ji DX, Vance RE, Price JV. Cell death and cell lysis are separable events during
837 pyroptosis. Cell Death Discov. 2017;3:17070. Epub 2017/11/18. doi: 10.1038/cddiscovery.2017.70.
838 PubMed PMID: 29147575; PubMed Central PMCID: PMCPMC5682879.
839 40. Fantuzzi G, Dinarello CA. Interleukin-18 and interleukin-1 beta: two cytokine substrates for ICE
840 (caspase-1). J Clin Immunol. 1999;19(1):1-11. doi: 10.1023/a:1020506300324. PubMed PMID:
841 10080100.
842 41. Galle M, Schotte P, Haegman M, Wullaert A, Yang HJ, Jin S, et al. The Pseudomonas aeruginosa
843 Type III secretion system plays a dual role in the regulation of caspase-1 mediated IL-1beta maturation. J
844 Cell Mol Med. 2008;12(5A):1767-76. Epub 2007/12/18. doi: 10.1111/j.1582-4934.2007.00190.x.
845 PubMed PMID: 18081695; PubMed Central PMCID: PMCPMC3918092.
846 42. Mohamed MF, Gupta K, Goldufsky JW, Roy R, Callaghan LT, Wetzel DM, et al. CrkII/Abl
847 phosphorylation cascade is critical for NLRC4 inflammasome activity and is blocked by Pseudomonas
848 aeruginosa ExoT. Nat Commun. 2022;13(1):1295. Epub 20220311. doi: 10.1038/s41467-022-28967-5.
849 PubMed PMID: 35277504.
850 43. Ince D, Sutterwala FS, Yahr TL. Secretion of Flagellar Proteins by the Pseudomonas aeruginosa
851 Type III Secretion-Injectisome System. J Bacteriol. 2015;197(12):2003-11. Epub 2015/04/08. doi:
852 10.1128/JB.00030-15. PubMed PMID: 25845843; PubMed Central PMCID: PMCPMC4438214.

853 44. Churchill MJ, Mitchell PS, Rauch I. Epithelial Pyroptosis in Host Defense. J Mol Biol.
854 2022;434(4):167278. Epub 20211008. doi: 10.1016/j.jmb.2021.167278. PubMed PMID: 34627788.
855 45. Lian H, Fang X, Li Q, Liu S, Wei Q, Hua X, et al. NLRP3 Inflammasome-Mediated Pyroptosis
856 Pathway Contributes to the Pathogenesis of Candida albicans Keratitis. Front Med (Lausanne).
857 2022;9:845129. Epub 20220406. doi: 10.3389/fmed.2022.845129. PubMed PMID: 35463001; PubMed
858 Central PMCID: PMCPMC9020473.
859 46. Zheng Q, Tan Q, Ren Y, Reinach PS, Li L, Ge C, et al. Hyperosmotic Stress-Induced TRPM2
860 Channel Activation Stimulates NLRP3 Inflammasome Activity in Primary Human Corneal Epithelial
861 Cells. Invest Ophthalmol Vis Sci. 2018;59(8):3259-68. doi: 10.1167/iovs.18-23965. PubMed PMID:
862 29971445.
863 47. Kelley N, Jeltema D, Duan Y, He Y. The NLRP3 Inflammasome: An Overview of Mechanisms
864 of Activation and Regulation. Int J Mol Sci. 2019;20(13). Epub 2019/07/10. doi: 10.3390/ijms20133328.
865 PubMed PMID: 31284572; PubMed Central PMCID: PMCPMC6651423.
866 48. Mariathasan S, Weiss DS, Newton K, McBride J, O'Rourke K, Roose-Girma M, et al. Cryopyrin
867 activates the inflammasome in response to toxins and ATP. Nature. 2006;440(7081):228-32. Epub
868 20060111. doi: 10.1038/nature04515. PubMed PMID: 16407890.
869 49. Hornung V, Bauernfeind F, Halle A, Samstad EO, Kono H, Rock KL, et al. Silica crystals and
870 aluminum salts activate the NALP3 inflammasome through phagosomal destabilization. Nature
871 Immunology. 2008;9(8):847-56. doi: 10.1038/ni.1631.
872 50. Kanneganti TD, Ozoren N, Body-Malapel M, Amer A, Park JH, Franchi L, et al. Bacterial RNA
873 and small antiviral compounds activate caspase-1 through cryopyrin/Nalp3. Nature. 2006;440(7081):233-
874 6. Epub 20060111. doi: 10.1038/nature04517. PubMed PMID: 16407888.
875 51. Kayagaki N, Wong MT, Stowe IB, Ramani SR, Gonzalez LC, Akashi-Takamura S, et al.
876 Noncanonical inflammasome activation by intracellular LPS independent of TLR4. Science.
877 2013;341(6151):1246-9. Epub 2013/07/28. doi: 10.1126/science.1240248. PubMed PMID: 23887873.
878 52. Bauernfried S, Scherr MJ, Pichlmair A, Duderstadt KE, Hornung V. Human NLRP1 is a sensor
879 for double-stranded RNA. Science. 2021;371(6528). Epub 2020/11/28. doi: 10.1126/science.abd0811.
880 PubMed PMID: 33243852.
881 53. Griswold AR, Huang HC, Bachovchin DA. The NLRP1 Inflammasome Induces Pyroptosis in
882 Human Corneal Epithelial Cells. Invest Ophthalmol Vis Sci. 2022;63(3):2. doi: 10.1167/iovs.63.3.2.
883 PubMed PMID: 35238869; PubMed Central PMCID: PMCPMC8899863.
884 54. Xu S, Liu X, Liu X, Shi Y, Jin X, Zhang N, et al. Wedelolactone ameliorates Pseudomonas
885 aeruginosa-induced inflammation and corneal injury by suppressing caspase-4/5/11/GSDMD-mediated
886 non-canonical pyroptosis. Exp Eye Res. 2021;211:108750. Epub 2021/09/06. doi:
887 10.1016/j.exer.2021.108750. PubMed PMID: 34481822.
888 55. Robertson DM, Li L, Fisher S, Pearce VP, Shay JW, Wright WE, et al. Characterization of
889 growth and differentiation in a telomerase-immortalized human corneal epithelial cell line. Invest
890 Ophthalmol Vis Sci. 2005;46(2):470-8. Epub 2005/01/27. doi: 10.1167/iovs.04-0528. PubMed PMID:
891 15671271.
892 56. Bitto NJ, Baker PJ, Dowling JK, Wray-McCann G, De Paoli A, Tran LS, et al. Membrane
893 vesicles from Pseudomonas aeruginosa activate the noncanonical inflammasome through caspase-5 in
894 human monocytes. Immunol Cell Biol. 2018;96(10):1120-30. Epub 20180814. doi: 10.1111/imcb.12190.
895 PubMed PMID: 30003588.
896 57. Reyes Ruiz VM, Ramirez J, Naseer N, Palacio NM, Siddarthan IJ, Yan BM, et al. Broad
897 detection of bacterial type III secretion system and flagellin proteins by the human NAIP/NLRC4
898 inflammasome. Proc Natl Acad Sci U S A. 2017;114(50):13242-7. Epub 20171127. doi:
899 10.1073/pnas.1710433114. PubMed PMID: 29180436; PubMed Central PMCID: PMCPMC5740664.
900 58. Thul PJ, Akesson L, Wiking M, Mahdessian D, Geladaki A, Ait Blal H, et al. A subcellular map
901 of the human proteome. Science. 2017;356(6340). Epub 20170511. doi: 10.1126/science.aal3321.
902 PubMed PMID: 28495876.

903 59. Kumar NG, Nieto V, Kroken AR, Jedel E, Grosser MR, Hallsten ME, et al. Pseudomonas
904 aeruginosa Can Diversify after Host Cell Invasion to Establish Multiple Intracellular Niches. mBio. 2022.
905 doi: 10.1128/mbio.02742-22.
906 60. Kaufman MR, Jia J, Zeng L, Ha U, Chow M, Jin S. Pseudomonas aeruginosa mediated apoptosis
907 requires the ADP-ribosylating activity of exoS. Microbiology (Reading). 2000;146 (Pt 10):2531-41. doi:
908 10.1099/00221287-146-10-2531. PubMed PMID: 11021928.
909 61. Vallis AJ, Finck-Barbancon V, Yahr TL, Frank DW. Biological effects of Pseudomonas
910 aeruginosa type III-secreted proteins on CHO cells. Infect Immun. 1999;67(4):2040-4. Epub 1999/03/20.
911 doi: 10.1128/IAI.67.4.2040-2044.1999. PubMed PMID: 10085057; PubMed Central PMCID:
912 PMCPMC96567.
913 62. Santos JC, Boucher D, Schneider LK, Demarco B, Dilucca M, Shkarina K, et al. Human GBP1
914 binds LPS to initiate assembly of a caspase-4 activating platform on cytosolic bacteria. Nat Commun.
915 2020;11(1):3276. Epub 2020/06/26. doi: 10.1038/s41467-020-16889-z. PubMed PMID: 32581219;
916 PubMed Central PMCID: PMCPMC7314798.
917 63. Kenny M, Schoen I. Violin SuperPlots: visualizing replicate heterogeneity in large data sets. Mol
918 Biol Cell. 2021;32(15):1333-4. Epub 2021/07/16. doi: 10.1091/mbc.E21-03-0130. PubMed PMID:
919 34264756.
920 64. Zamyatina A, Heine H. Lipopolysaccharide Recognition in the Crossroads of TLR4 and Caspase-
921 4/11 Mediated Inflammatory Pathways. Front Immunol. 2020;11:585146. Epub 20201127. doi:
922 10.3389/fimmu.2020.585146. PubMed PMID: 33329561; PubMed Central PMCID: PMCPMC7732686.
923 65. Kobayashi T, Ogawa M, Sanada T, Mimuro H, Kim M, Ashida H, et al. The Shigella OspC3
924 effector inhibits caspase-4, antagonizes inflammatory cell death, and promotes epithelial infection. Cell
925 Host Microbe. 2013;13(5):570-83. Epub 2013/05/21. doi: 10.1016/j.chom.2013.04.012. PubMed PMID:
926 23684308.
927 66. Li Z, Liu W, Fu J, Cheng S, Xu Y, Wang Z, et al. Shigella evades pyroptosis by arginine ADP-
928 riboxanation of caspase-11. Nature. 2021. Epub 2021/10/22. doi: 10.1038/s41586-021-04020-1. PubMed
929 PMID: 34671164.
930 67. Goers L, Kim K, Canning PJ, Stedman TC, Mou X, Ernst NH, et al. *Shigella* IpaH9.8 limits
931 GBP1-dependent LPS release from intracytosolic bacteria to suppress caspase-4 activation. bioRxiv.
932 2022:2022.11.14.516511. doi: 10.1101/2022.11.14.516511.
933 68. Knodler LA, Nair V, Steele-Mortimer O. Quantitative assessment of cytosolic Salmonella in
934 epithelial cells. PLoS One. 2014;9(1):e84681. Epub 2014/01/09. doi: 10.1371/journal.pone.0084681.
935 PubMed PMID: 24400108; PubMed Central PMCID: PMCPMC3882239.
936 69. Alaoui-El-Azher M, Jia J, Lian W, Jin S. ExoS of Pseudomonas aeruginosa induces apoptosis
937 through a Fas receptor/caspase 8-independent pathway in HeLa cells. Cell Microbiol. 2006;8(2):326-38.
938 doi: 10.1111/j.1462-5822.2005.00624.x. PubMed PMID: 16441442.
939 70. Jia J, Alaoui-El-Azher M, Chow M, Chambers TC, Baker H, Jin S. c-Jun NH2-terminal kinase-
940 mediated signaling is essential for Pseudomonas aeruginosa ExoS-induced apoptosis. Infect Immun.
941 2003;71(6):3361-70. doi: 10.1128/IAI.71.6.3361-3370.2003. PubMed PMID: 12761120; PubMed Central
942 PMCID: PMCPMC155783.
943 71. Jia J, Wang Y, Zhou L, Jin S. Expression of Pseudomonas aeruginosa toxin ExoS effectively
944 induces apoptosis in host cells. Infect Immun. 2006;74(12):6557-70. Epub 2006/09/13. doi:
945 10.1128/IAI.00591-06. PubMed PMID: 16966406; PubMed Central PMCID: PMCPMC1698105.
946 72. Taabazuing CY, Okondo MC, Bachovchin DA. Pyroptosis and Apoptosis Pathways Engage in
947 Bidirectional Crosstalk in Monocytes and Macrophages. Cell Chem Biol. 2017;24(4):507-14 e4. Epub
948 20170406. doi: 10.1016/j.chembiol.2017.03.009. PubMed PMID: 28392147; PubMed Central PMCID:
949 PMCPMC5467448.
950 73. Vanaja SK, Russo AJ, Behl B, Banerjee I, Yankova M, Deshmukh SD, et al. Bacterial Outer
951 Membrane Vesicles Mediate Cytosolic Localization of LPS and Caspase-11 Activation. Cell.
952 2016;165(5):1106-19. Epub 20160505. doi: 10.1016/j.cell.2016.04.015. PubMed PMID: 27156449;
953 PubMed Central PMCID: PMCPMC4874922.

954 74. Deng M, Tang Y, Li W, Wang X, Zhang R, Zhang X, et al. The Endotoxin Delivery Protein
955 HMGB1 Mediates Caspase-11-Dependent Lethality in Sepsis. Immunity. 2018;49(4):740-53 e7. Epub
956 20181009. doi: 10.1016/j.immuni.2018.08.016. PubMed PMID: 30314759; PubMed Central PMCID:
957 PMCPMC6300139.
958 75. Balakrishnan A, Karki R, Berwin B, Yamamoto M, Kanneganti TD. Guanylate binding proteins
959 facilitate caspase-11-dependent pyroptosis in response to type 3 secretion system-negative Pseudomonas
960 aeruginosa. Cell Death Discov. 2018;4:3. Epub 20180627. doi: 10.1038/s41420-018-0068-z. PubMed
961 PMID: 30062052; PubMed Central PMCID: PMCPMC6060091.
962 76. Sato H, Frank DW. ExoU is a potent intracellular phospholipase. Mol Microbiol.
963 2004;53(5):1279-90. Epub 2004/09/25. doi: 10.1111/j.1365-2958.2004.04194.x. PubMed PMID:
964 15387809.
965 77. Luchetti G, Roncaioli JL, Chavez RA, Schubert AF, Kofoed EM, Reja R, et al. Shigella ubiquitin
966 ligase IpaH7.8 targets gasdermin D for degradation to prevent pyroptosis and enable infection. Cell Host
967 Microbe. 2021. Epub 2021/09/08. doi: 10.1016/j.chom.2021.08.010. PubMed PMID: 34492225.
968 78. Barbieri JT, Sun J. Pseudomonas aeruginosa ExoS and ExoT. Rev Physiol Biochem Pharmacol.
969 2004;152:79-92. Epub 2004/09/18. doi: 10.1007/s10254-004-0031-7. PubMed PMID: 15375697.
970 79. Grandjean T, Boucher A, Thepaut M, Monlezun L, Guery B, Faudry E, et al. The human NAIP-
971 NLRC4-inflammasome senses the Pseudomonas aeruginosa T3SS inner-rod protein. Int Immunol.
972 2017;29(8):377-84. Epub 2017/10/11. doi: 10.1093/intimm/dxx047. PubMed PMID: 28992059.
973 80. Sun Y, Karmakar M, Taylor PR, Rietsch A, Pearlman E. ExoS and ExoT ADP ribosyltransferase
974 activities mediate Pseudomonas aeruginosa keratitis by promoting neutrophil apoptosis and bacterial
975 survival. J Immunol. 2012;188(4):1884-95. Epub 2012/01/18. doi: 10.4049/jimmunol.1102148. PubMed
976 PMID: 22250085; PubMed Central PMCID: PMCPMC3273577.
977 81. Urbanowski ML, Brutinel ED, Yahr TL. Translocation of ExsE into Chinese hamster ovary cells
978 is required for transcriptional induction of the Pseudomonas aeruginosa type III secretion system. Infect
979 Immun. 2007;75(9):4432-9. Epub 2007/07/20. doi: 10.1128/IAI.00664-07. PubMed PMID: 17635873;
980 PubMed Central PMCID: PMCPMC1951186.
981 82. Sanjana NE, Shalem O, Zhang F. Improved vectors and genome-wide libraries for CRISPR
982 screening. Nat Methods. 2014;11(8):783-4. doi: 10.1038/nmeth.3047. PubMed PMID: 25075903;
983 PubMed Central PMCID: PMCPMC4486245.
984 83. Schmidt T, Schmid-Burgk JL, Hornung V. Synthesis of an arrayed sgRNA library targeting the
985 human genome. Sci Rep. 2015;5:14987. Epub 20151008. doi: 10.1038/srep14987. PubMed PMID:
986 26446710; PubMed Central PMCID: PMCPMC4597219.
987

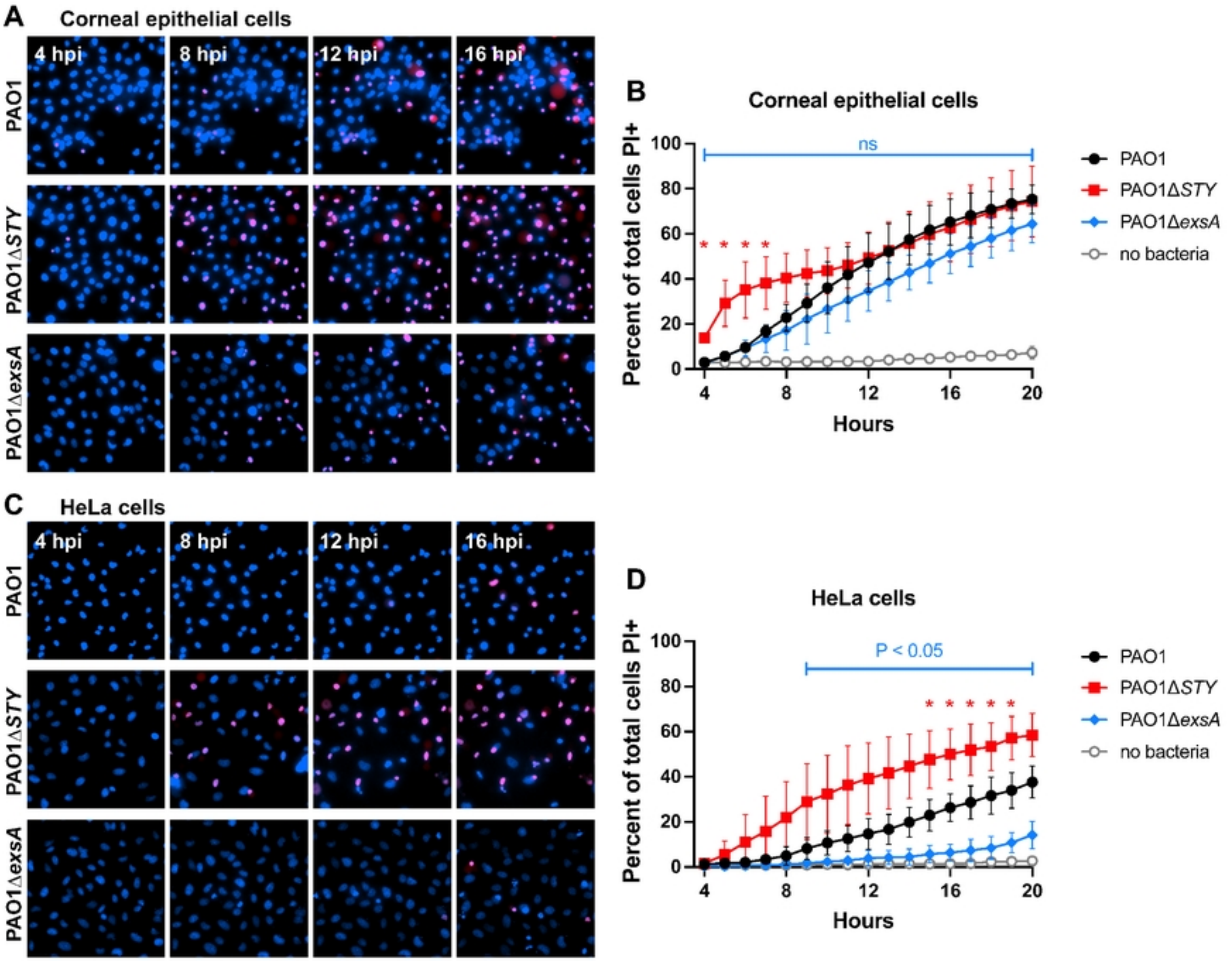
A
Corneal epithelial cells
4 hpi
8 hpi
12 hpi
16 hpi
PAO1
PAO1ΔSTY
PAO1ΔexsA
B
Corneal epithelial cells
Percent of total cells PI+
ns
Hours
PAO1
PAO1ΔSTY
PAO1ΔexsA
no bacteria
C
HeLa cells
D
HeLa cells
P < 0.05

Figure 1

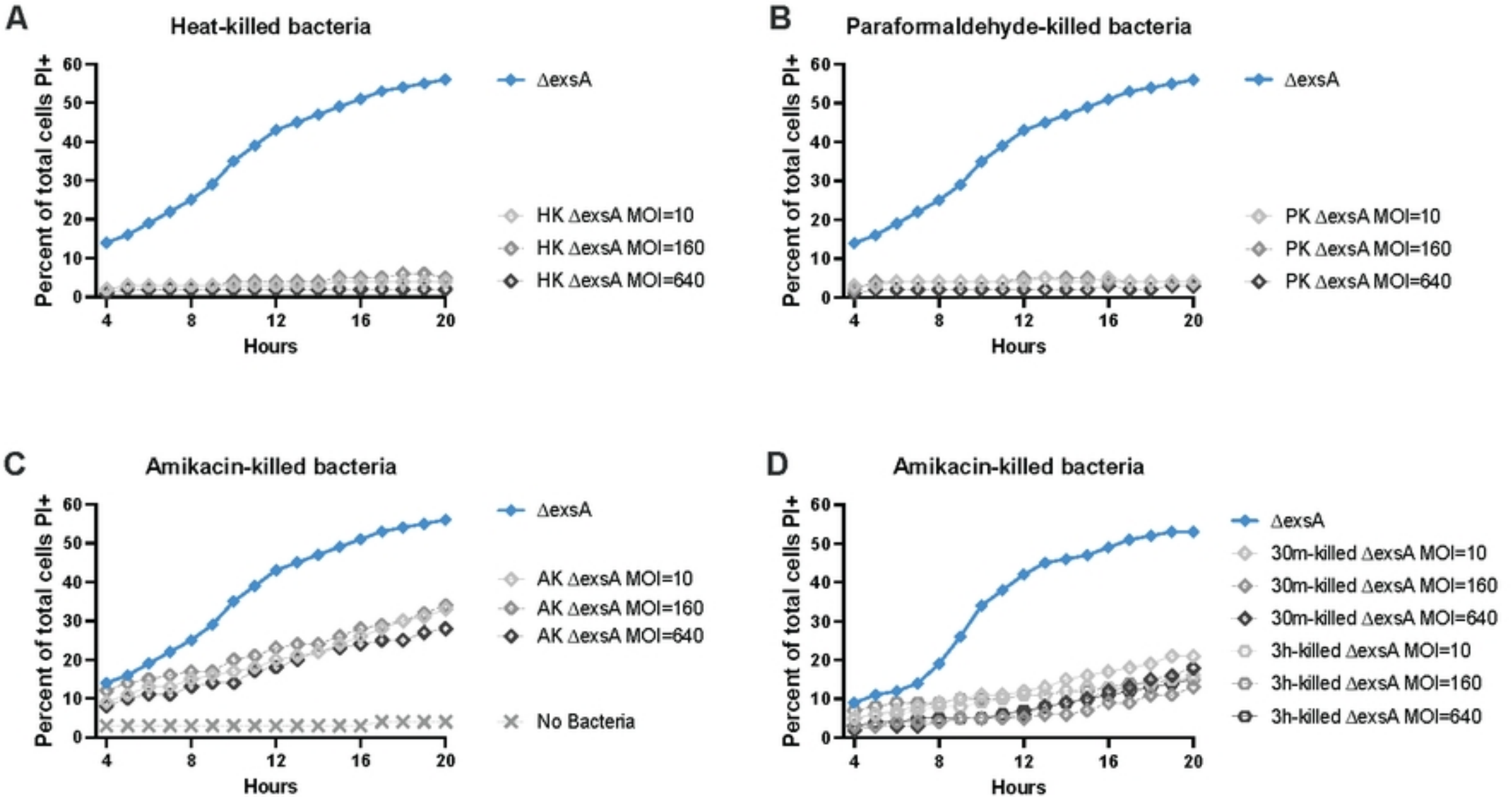
A
Heat-killed bacteria
Percent of total cells PI+
Hours
ΔexsA
HK ΔexsA MOI=10
HK ΔexsA MOI=160
HK ΔexsA MOI=640
B
Paraformaldehyde-killed bacteria
Percent of total cells PI+
Hours
ΔexsA
PK ΔexsA MOI=10
PK ΔexsA MOI=160
PK ΔexsA MOI=640
C
Amikacin-killed bacteria
Percent of total cells PI+
Hours
ΔexsA
AK ΔexsA MOI=10
AK ΔexsA MOI=160
AK ΔexsA MOI=640
No Bacteria
D
Amikacin-killed bacteria
Percent of total cells PI+
Hours
ΔexsA
30m-killed ΔexsA MOI=10
30m-killed ΔexsA MOI=160
30m-killed ΔexsA MOI=640
3h-killed ΔexsA MOI=10
3h-killed ΔexsA MOI=160
3h-killed ΔexsA MOI=640

Figure 2

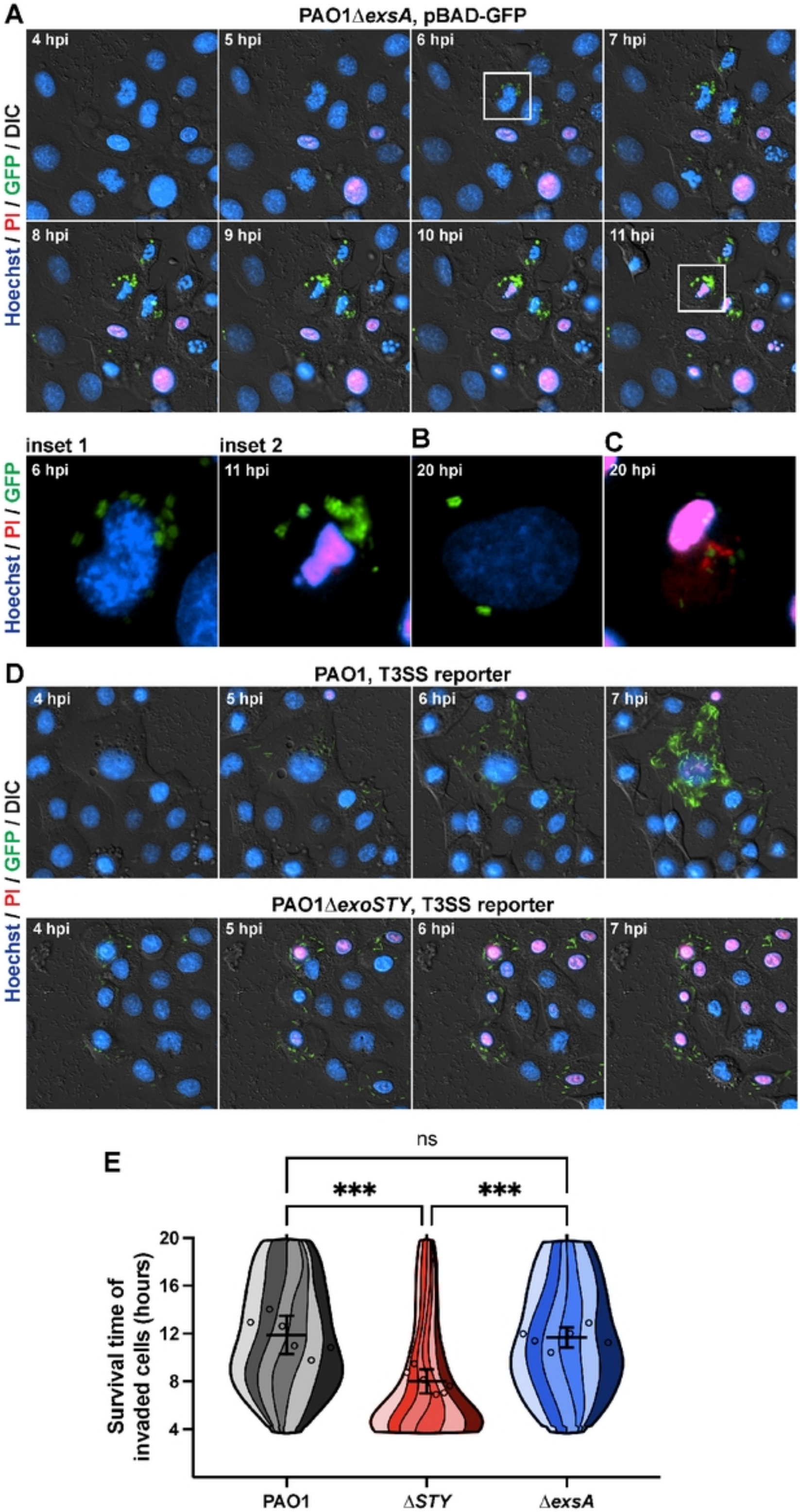
A
PAO1ΔexsA, pBAD-GFP
4 hpi
5 hpi
6 hpi
7 hpi
8 hpi
9 hpi
10 hpi
11 hpi
Hoechst / PI / GFP / DIC
inset 1
inset 2
B
C
6 hpi
11 hpi
20 hpi
20 hpi
Hoechst / PI / GFP
D
PAO1, T3SS reporter
4 hpi
5 hpi
6 hpi
7 hpi
Hoechst / PI / GFP / DIC
PAO1ΔexoSTY, T3SS reporter
4 hpi
5 hpi
6 hpi
7 hpi
Hoechst / PI / GFP
E
ns
***
***
Survival time of invaded cells (hours)
20
16
12
8
4
PAO1
ΔSTY
ΔexsA

Figure 3

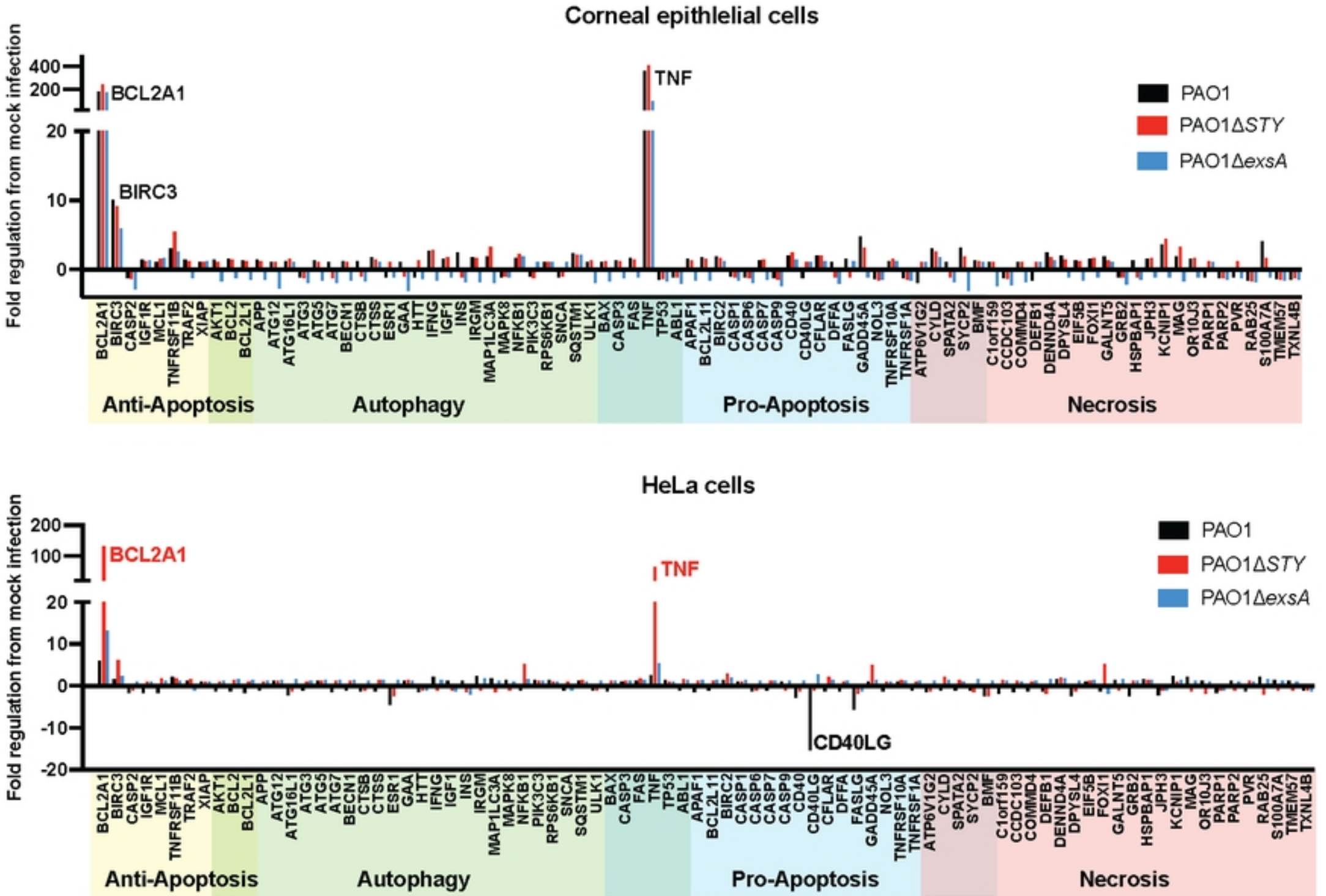
Corneal epithlelial cells
Fold regulation from mock infection
400
200
20
10
0
BCL2A1
BIRC3
TNF
PAO1
PAO1ΔSTY
PAO1ΔexsA
BCL2A1 BIRC3 CASP2 IGF1R MCL1 TNFRSF11B TRAF2 XIAP AKT1 BCL2 BCL2L1 APP ATG12 ATG16L1 ATG3 ATG5 ATG7 BECN1 CTSB CTSS ESR1 GAA HTT IFNG IGF1 INS IRGM MAP1LC3A MAPK8 NFKB1 PIK3C3 RPS6KB1 SNCA SQSTM1 ULK1 BAX CASP3 FAS TNF TP53 ABL1 APAF1 BCL2L11 BIRC2 CASP1 CASP6 CASP7 CASP9 CD40 CD40LG CFLAR DFFA FASLG GADD45A NOL3 TNFRSF10A TNFRSF1A ATP6V1G2 CYLD SPATA2 SYCP2 BMF C1orf159 CCDC103 COMMD4 DEFB1 DENND4A DPYSL4 EIF5B FOXI1 GALNT5 GRB2 HSPBAP1 JPH3 KCNIP1 MAG OR10J3 PARP1 PARP2 PVR RAB25 S100A7A TMEM57 TXNL4B
Anti-Apoptosis
Autophagy
Pro-Apoptosis
Necrosis
HeLa cells
Fold regulation from mock infection
200
100
20
10
0
-10
-20
BCL2A1
TNF
CD40LG
PAO1
PAO1ΔSTY
PAO1ΔexsA
BCL2A1 BIRC3 CASP2 IGF1R MCL1 TNFRSF11B TRAF2 XIAP AKT1 BCL2 BCL2L1 APP ATG12 ATG16L1 ATG3 ATG5 ATG7 BECN1 CTSB CTSS ESR1 GAA HTT IFNG IGF1 INS IRGM MAP1LC3A MAPK8 NFKB1 PIK3C3 RPS6KB1 SNCA SQSTM1 ULK1 BAX CASP3 FAS TNF TP53 ABL1 APAF1 BCL2L11 BIRC2 CASP1 CASP6 CASP7 CASP9 CD40 CD40LG CFLAR DFFA FASLG GADD45A NOL3 TNFRSF10A TNFRSF1A ATP6V1G2 CYLD SPATA2 SYCP2 BMF C1orf159 CCDC103 COMMD4 DEFB1 DENND4A DPYSL4 EIF5B FOXI1 GALNT5 GRB2 HSPBAP1 JPH3 KCNIP1 MAG OR10J3 PARP1 PARP2 PVR RAB25 S100A7A TMEM57 TXNL4B
Anti-Apoptosis
Autophagy
Pro-Apoptosis
Necrosis

Figure 4

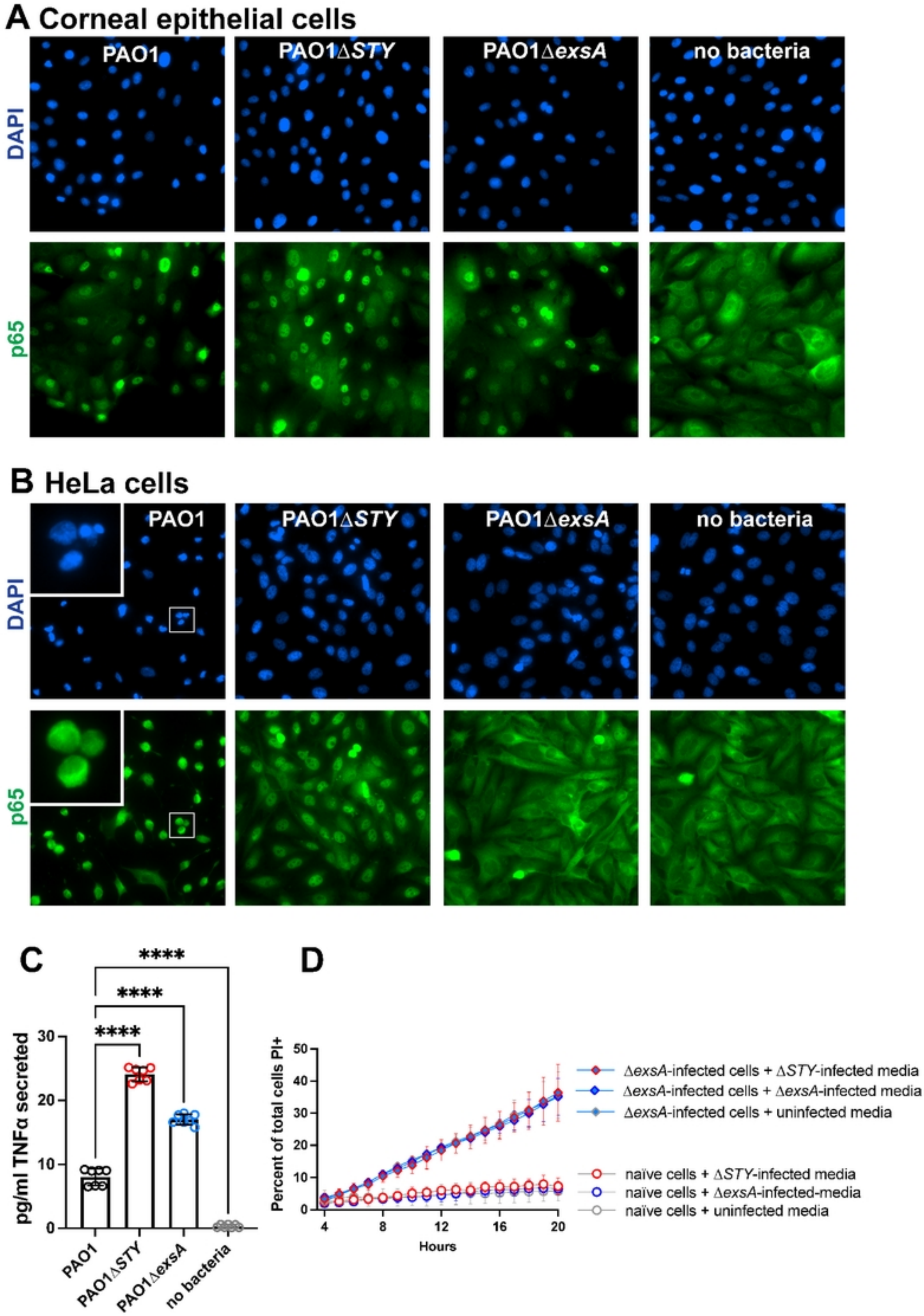
A Corneal epithelial cells
PAO1
PAO1ΔSTY
PAO1ΔexsA
no bacteria
DAPI
p65
B HeLa cells
PAO1
PAO1ΔSTY
PAO1ΔexsA
no bacteria
DAPI
p65
C
****
****
****
pg/ml TNFα secreted
30
20
10
0
PAO1
PAO1ΔSTY
PAO1ΔexsA
no bacteria
D
Percent of total cells PI+
50
40
30
20
10
0
4
8
12
16
20
Hours
ΔexsA-infected cells + ΔSTY-infected media
ΔexsA-infected cells + ΔexsA-infected media
ΔexsA-infected cells + uninfected media
naïve cells + ΔSTY-infected media
naïve cells + ΔexsA-infected-media
naïve cells + uninfected media

Figure 5

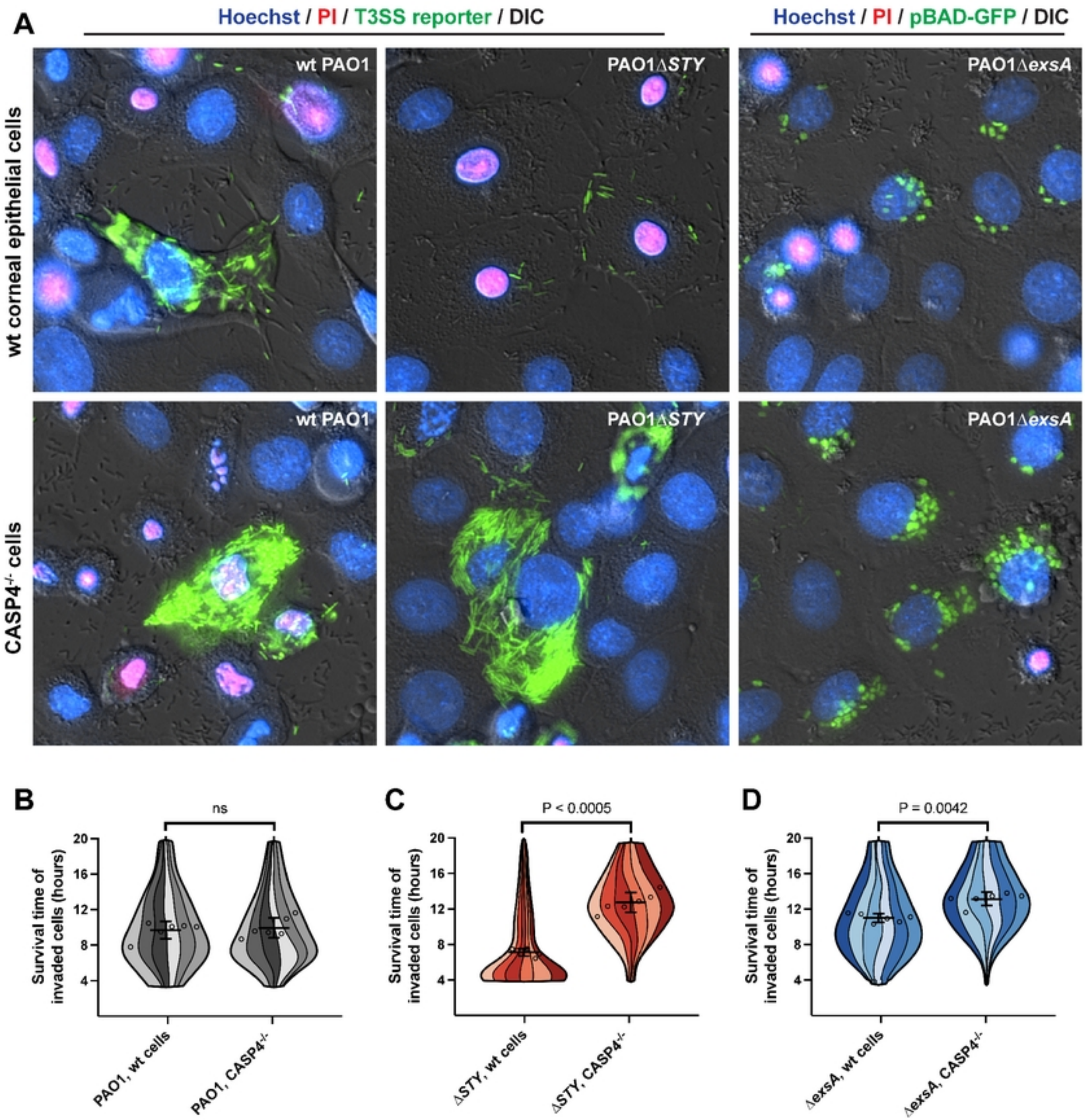
A
Hoechst / PI / T3SS reporter / DIC
Hoechst / PI / pBAD-GFP / DIC
wt corneal epithelial cells
CASP4-/- cells
wt PAO1
PAO1ΔSTY
PAO1ΔexsA
B
C
D
ns
P < 0.0005
P = 0.0042
Survival time of invaded cells (hours)
20
16
12
8
4
PAO1, wt cells
PAO1, CASP4-/-
ΔSTY, wt cells
ΔSTY, CASP4-/-
ΔexsA, wt cells
ΔexsA, CASP4-/-

Figure 6

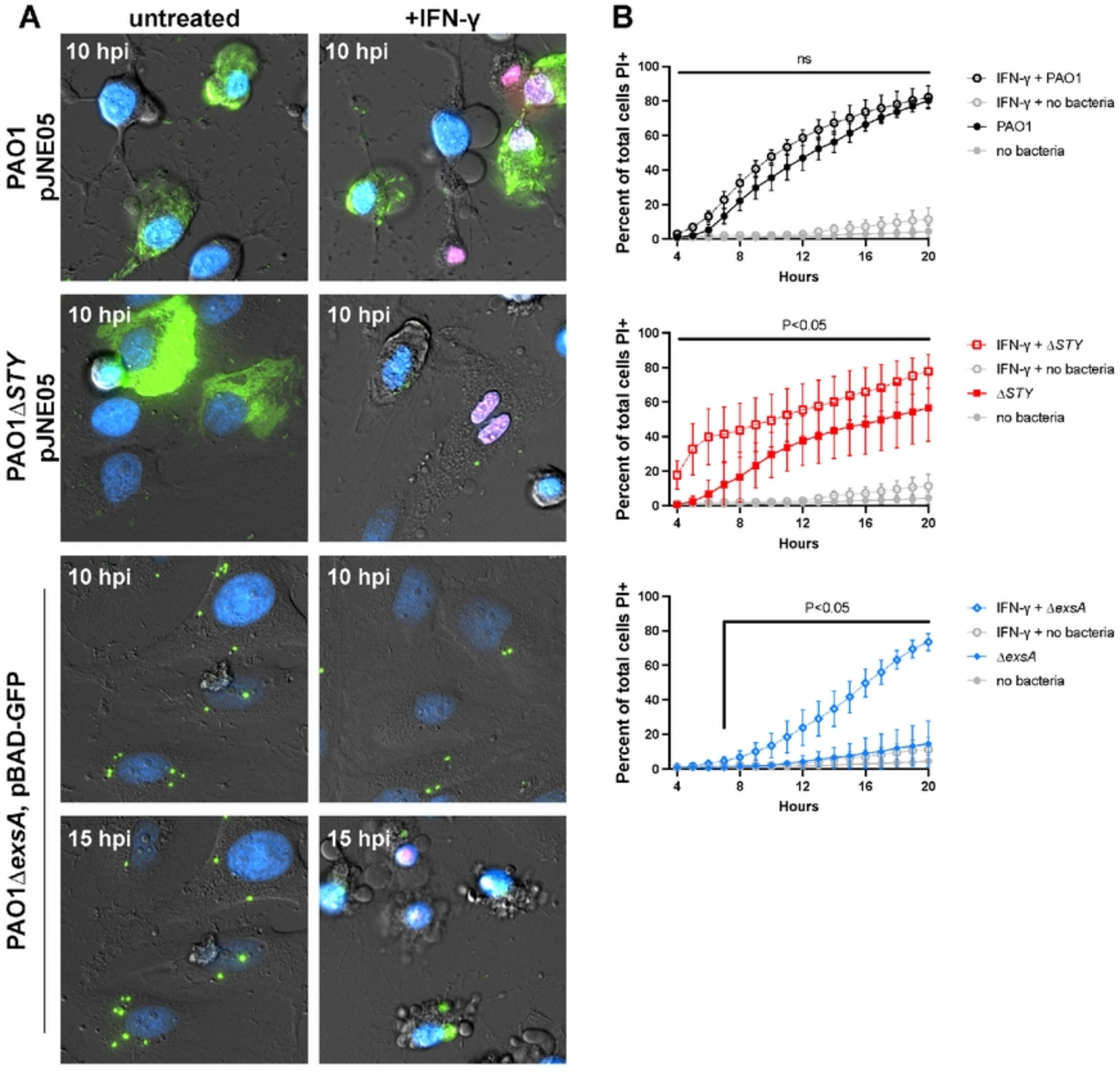
A
untreated
+IFN-γ
PAO1 pJNE05
PAO1ΔSTY pJNE05
PAO1ΔexsA, pBAD-GFP
10 hpi
15 hpi
B
Percent of total cells PI+
Hours
ns
P<0.05
IFN-γ + PAO1
IFN-γ + no bacteria
PAO1
no bacteria
IFN-γ + ΔSTY
ΔSTY
IFN-γ + ΔexsA
ΔexsA

Figure 7